

Degree Project in Technology

First cycle, 15 credits

Crash Properties of Aluminium Extrusions

Investigation of Possible Ductility Parameters and Correlations from Tensile Tests and Compression Tests of Crash Boxes for the Vehicular Industry

ZOË PETRÉN, HANNES SCHÖNQVIST



Abstract

The use of extruded aluminium profiles in the vehicle industry is increasing. One type of aluminium extrusions in cars are crash boxes, which absorb energy at low-velocity crashes. To ensure the quality of the material, the crash boxes are tested through compression tests and tensile tests. The compression tests are costly with regards to both material and time but serve an important purpose; to allow an evaluation of the degree of cracking, which needs to be low. Based on an internal study by Hydro Extrusion Sweden AB in Finspång, whom this study is conducted in collaboration with, the purpose of this report is to correlate the results of compression- and tensile tests in order to in the future eliminate the need for compression tests. Five crash box profiles of alloy 6063 were extruded and treated with different quenching methods and ageing cycles. Through compression- and tensile testing, the alloy's properties were evaluated to find suitable ductility parameters that may be used to predict the cracking behaviour of a crash box depending on the ageing cycle. According to the internal study, it has been proven to work for a water-quenched 6063-alloy and using our results concluded that it is also possible with an air-cooled 6063-alloy. Furthermore, it is concluded that if the cracking behaviour of a crash box of the 6063-alloy is to be predicted, a proper model that takes the box's geometry into account should be used.

Sammanfattning

Extruderade aluminiumprofiler blir allt vanligare inom fordonsindustrin. En typ av sådana aluminiumprofiler i bilar är krockboxar som tar upp energi vid låghastighetskrockar. För att säkerställa materialets kvalitet testas krockboxarna med dragprov och kompressionstest. Dessa kompressionstest är material- och tidskrävande men de behövs för utvärdering av graden av sprickning som inte får vara för stor. Baserat på en intern studie vid Hydro Extrusion Sweden AB i Finspång, som detta projekt görs i samband med, är syftet med detta arbete att korrelera resultat från kompressionstest och dragprov för att på lång sikt kunna eliminera behovet av kompressionstest. Fem krockboxprofiler av legeringen 6063 extruderades och behandlades med olika släckningsmetoder och åldringscykler. Genom kompressionstester och dragprov korrelerades legeringens egenskaper med varandra för att utvärdera lämplighet för duktilitetsparametrar som sedan undersöktes i syfte att kunna förutspå krockboxens sprickningsbeteende beroende på åldringscykel. Enligt den interna undersökningen har det påvisats att det fungerar med en vattenkyld 6063-legering och utifrån vårt resultat kan slutsatsen dras att det också fungerar för en luftkyld 6063-legering. Dessutom kan slutsatsen dras att om sprickbeteendet hos en krockbox av 6063-legering ska förutspås bör en modell som tar hänsyn till krockboxens geometri användas.

Nomenclature

MCF - mean crush force [kN]

S_0 - original cross-section area of tensile test [mm²]

S_u - fracture surface of tensile test measured as the horizontal projection [mm²]

Z - area reduction defined as $Z = \frac{S_0 - S_u}{S_0} \cdot 100$ [%]

ϵ_f - true fracture strain estimated as $\epsilon_f = \ln\left(\frac{S_0}{S_u}\right) \cdot 100$ [%]

R_m - ultimate tensile strength [MPa]

$R_{p0.2}$ - yield strength [MPa]

R_f - fracture stress, defined as the last point of stress recorded in tensile test [MPa]

T4 - no ageing

Table of contents

1. Introduction	1
1.1 Aluminium in the vehicular industry	1
1.2 Hydro Extrusion Sweden	1
1.3 Problem formulation	1
1.4 Related works	2
1.5 Project goals	2
2. 6063, the properties of aluminium extrusions related to crash properties and previous studies	3
2.1 Aluminium and the 6063-alloy	3
2.2 The extrusion process of Hydro Extrusion Sweden AB	4
2.2.1 Casting	4
2.2.2 Homogenisation	4
2.2.3 Extrusion	5
2.2.4 Quenching and Stretching	5
2.2.5 Ageing	6
2.3 Crash boxes, relevant properties and the testing of them	6
2.3.1 Crash performance and tensile testing	6
2.3.2 Theory of relevant properties	7
2.3.3 Previous studies	7
3. Method	10
3.1 Extrusion, quenching and ageing	10
3.2 Compression test	11
3.3 Tensile test	13
3.4 Area reduction measurements and microscopy	13
3.5 Implementation of calculations and plots	14
4. Results	15
4.1 Cooling rate of extrusions	15
4.2 Tensile test	16
4.3 Compression test	19
4.4 Evaluation of ductility parameters	21
4.5 Microstructural observations	28
5. Discussion	29
5.1 Evaluation of results	29
5.1.1 Tensile test results	29
5.1.2 Grade of Cracking and True Fracture Strain	29
5.1.3 Evaluation of ductility parameters	30
5.1.4 The relation between ductility, strength and ageing time	30
5.1.5 Correlation between MCF and Rm, MCF and Rpo.2	31
5.1.6 Correlation between Rm-Rf and Z	31

5.2 Comments on production and measurement methods	32
5.3 The Aluminium industry and CO ₂ emissions	33
6. Conclusions	35
7. Recommendations	36
8. Acknowledgements	37
9. References	38
Appendix	A - 1
Appendix A: Microscopy images	A - 1

1. Introduction

1.1 Aluminium in the vehicular industry

For vehicle manufacturers to remain competitive in their market the cars they make have to be as light as possible whilst remaining safe for the passengers. Consequently, the use of aluminium when constructing the automotive body is very common, as the metal has a high strength-to-density-relation and high ductility [1]. The use of aluminium alloys in the vehicular industry is predicted to increase by about 50 kg per constructed vehicle by 2030. This is especially due to the need for aluminium in electrification along with the general trend that causes new car models to grow bigger [2]. Aluminium extrusions in cars are, among several other structural details, used as energy-absorbing components [3]. An example, crash boxes, are thin-walled metal tubes situated in the front of the car, one on each side. The endeavour is that the crash box will, in case of a low-velocity crash, deform in such a manner that it absorbs a sufficient amount of energy to minimise the damage done to the passengers [4].

1.2 Hydro Extrusion Sweden

Hydro is an aluminium and energy company operating in 40 different countries and has 33 000 employees (2023) [5]. At Hydro's plants in Sweden, in Finspång and Vetlanda, the focus is on the extrusion of aluminium profiles and building systems. This bachelor thesis is performed in cooperation with Hydro Extrusion Sweden AB at the plant in Finspång. Hydro Extrusions Finspång have the facilities to extrude big profiles, a research & development centre, and offers solutions for machining, assembly and coatings. They also have a remelting plant with the possibility to remelt even lacquered scrap and scrap from the end customer [6], [7].

1.3 Problem formulation

It is of the highest importance that the mechanical properties of crash boxes and other components with crash-dampening functions are accurately tested and ensured by the manufacturer. The relevant properties for a component in means of crash performance are commonly called crash properties. Crash properties of extruded aluminium crash boxes are measured by compression tests whilst measuring the amount of energy that the specimen can absorb during compression. The crash properties are also judged by visual inspection of the specimen after compression. The visual inspection aims to determine the level of cracking and to evaluate the folding behaviour, where a bellows-shaped result is to be preferred. However, there is a will to investigate compression tests alongside tensile tests in order to find more kinds of subjective test parameters that may indicate the crash properties of the material. Resulting in the ability to draw more conclusions from

simpler and less time-consuming tests with less metal scrap as a result. This problem is originally formulated by Hydro Extrusion Sweden AB.

1.4 Related works

Several studies have investigated mechanical testing of actual crash box models or extruded thin-walled tubes, relating the results to the microstructure and production parameters such as cooling rate after extrusion and ageing of the specimens. In this project, a technical memo by J. Mendoza [3] has been an important source for previous studies, where a thorough literature study has been made. Some of these previous studies regarding alloys from the 6XXX aluminium alloy series have been studied in this project and are mentioned in this report to get a deeper understanding of the whole picture [8], [9], [10], [11]. It should be emphasised that other investigations of correlations between tensile- and crash properties have been done. The literature study by Mendoza [3] mentions results from a couple of articles describing correlations between tensile test parameters and bending test or limiting-dome height respectively [12], [13]. This project stems from a similar field of research but has a different kind of focus.

In an internal investigation at Hydro Extrusion Sweden AB made by A. Assisi, tensile tests were performed on samples from an extruded crash box model in aluminium alloy 6063, that were water-quenched post-extrusion and treated with different ageing programs. A measurement of the area reduction from the necking was also done and considered as a ductility parameter. It has been found that there is a strong correlation between the area reduction during necking and other parameters such as the difference between the ultimate tensile strength and the last recorded point of stress before fracture. This difference was found to increase with increased ageing time in the same manner as the area reduction/ductility increases with increased over ageing [14]. A study by Parson et al. has among other parameters investigated and found a correlation between true fracture strain and the level of cracking along with a linear relation between the mean crush force (absorbed energy during compression) and ultimate tensile strength [9], [15].

1.5 Project goals

This project aims to further investigate the relations between different tensile- and compression test results. This is done by partly replicating the experiments of the internal investigation from Hydro Extrusion Sweden AB [14] and by exploring whether the correlation still applies when the extrusion is air-cooled post-extrusion. Compression tests are performed as well, comparing the results from the tensile tests in a similar manner as in the study by Parson et al. [9], [15]. The experiments of this investigation were done at the Hydro Extrusion Sweden AB plant in Finspång with technical and material resources provided by and in cooperation with the company.

2. 6063, the properties of aluminium extrusions related to crash properties and previous studies

2.1 Aluminium and the 6063-alloy

Aluminium alloys are divided into groups depending on their composition. The so-called 6XXX series consists of aluminium alloys with different amounts of silicon and magnesium and is considered one of the most promising groups of materials that may be used in the body of vehicles [1]. In general, this is because of the alloys' corrosion resistance, immunity to stress-corrosion-cracking, relatively high strength, weldability and tremendous formability. This combination of properties allows in turn the alloys of the 6XXX-series to be wrought in a series of ways, including extrusion, which is the production method examined in this report.

When considering a 6XXX alloy, we may regard the quasi-binary system, Al-Mg₂Si (Figure 1), as Mg₂Si precipitates are one of the largest contributions to the strength of the alloy [16]. However, an increase in Mg₂Si precipitates also leads to more friction during the extrusion process, forcing the extrusion speed to be reduced to maintain the quality of the product [17]. Furthermore, three subcategories may be constructed of the 6XXX-series. The first category consists of alloys with a nearly 1:1 relationship between the Si- and Mg-contents with a deviation of about 0.8% to 1.2% of the total composition. The two other categories consist of alloys over 1.4% Si where precipitates consisting of pure Si may be formed alongside Mg₂Si [16].

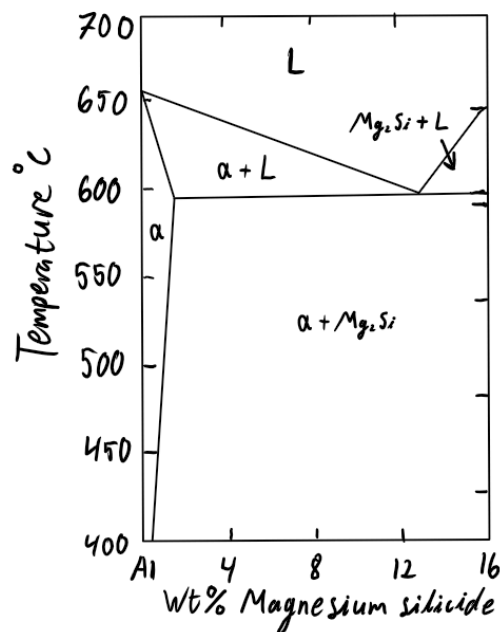


Fig. 1 Al-Mg₂Si phase diagram

The most used 6XXX-series alloy for extrusion processes is the 6063-alloy which has been called “the bread and butter for the extrusion industry” [17]. Generally, 6063 alloys are alloyed with 0.20-0.6 wt% Si, 0.45-0.9 wt% Mg and a maximum of 0.35 wt% Fe where more specific compositions regarding Si, Mg and Fe along with other minor alloying elements are set depending on the producer and the product [16], [18]. 6063-alloys are because of the similar content of Si and Mg part of the first aforementioned category of 6XXX-series alloys, which means that the material has great extrudability, a term for a combination of properties that is beneficial for extrusion productivity. More specifically, the similar amount of Si and Mg along with a generally low content of other alloying elements result in a low quench sensitivity and higher extrusion speeds. Quench sensitivity is a term describing the instability of a supersaturated solid. Extruded profiles of an alloy that have low quench sensitivity may be quenched directly after extrusion in order to achieve proper supersaturation of Mg_2Si . Usually, if the quench sensitivity of a material that is to be extruded is high, precipitates tend to form in the grain boundaries directly after extrusion. Consequently, if the cooling of this material is not fast enough to inhibit the formation of precipitates, a separate production step needs to be added where the extrusions are solution-treated and quenched to achieve proper supersaturation before ageing [16].

2.2 The extrusion process of Hydro Extrusion Sweden AB

2.2.1 Casting

To extrude an aluminium profile, the billets which are used as the starting unit of extrusion need to be made. After a melt with the proper amount of each component has been made through the process of melting scrap and primary aluminium, alloying and degassing, the melt is cast into billets. At Hydro Extrusion Sweden AB, direct casting is utilised where casting speed, temperature and melt depth are monitored and controlled with a lowering rate and continuous water cooling. It is important to consider the defects that may appear during casting as they may compromise an extruded profile [19].

2.2.2 Homogenisation

A large quantity of the issues that may be found in an extruded profile derives from a heterogeneous microstructure where, in the case of 6XXX-alloys, Mg_2Si -precipitates are not sufficiently dispersed and in a solid solution. The heterogeneous microstructure is mainly caused by microsegregations and the formation of Mg_2Si during casting and may be turned homogeneous through homogenisation [17]. Moreover, it is of interest to achieve a completely homogeneous solid solution before extrusion as precipitates may cause weaker and more quench sensitive profiles that are also more prone to recrystallize during extrusion [19].

2.2.3 Extrusion

During direct extrusion, the billet is after the homogenisation process loaded into a container that holds approximately 480°C, with a slight heat gradient front to back to prepare the billet for extrusion with an increased flowability. The billet is then pressed through a die that may consist of one or two parts depending on whether the extrusion is to be hollow or not. During this extrusion process, the profile will hold an approximate temperature of 580°C. Alas, there are plenty of different extrusion defects that may occur and do so unless proper measures are taken. If the entire billet is put through the die, defects originating from the billets' end pieces might surge into the extruded profiles. Therefore, the last part of the cast billet is cut off by the so-called discard. Furthermore, defects such as various surface defects and pipe-formation may occur due to contaminations, inadequate lubrication, too high extrusion speed and design flaws [19].

The degree of recrystallisation as an effect of extrusion is a very important aspect when it comes to the processing of 6XXX alloys. Whether or not recrystallisation is desired, and to which degree, is closely related to the alloying composition as a large content of alloying elements inhibits recrystallisation. In highly alloyed aluminium, recrystallisation is very undesirable as the degree of recrystallisation will be low which leads to larger grains and therefore a weaker and more brittle material. Usually, recrystallisation of these alloys occurs in the outermost surface layer of the material, leaving the core untouched. On the other hand, low alloyed aluminium, including the 6063-alloy, inevitably recrystallise during extrusion which is generally not an issue as the grain structure retained generally is very fine [17].

2.2.4 Quenching and Stretching

After a profile has exited the die it is to be quenched in air or water. Generally, the initial factor to consider when choosing which medium an aluminium alloy is cooled in depends on the alloy's quench sensitivity. If the cooling rate is too low in relation to the quench sensitivity, undesired precipitates will form. Quenching in water will result in a greater final strength after ageing as the supersaturation of Mg_2Si will be greater the faster the temperature reaches temperatures below the critical temperature, which is a threshold beneath which no significant microstructural changes occur. However, water quenching may require extra space for equipment that need water access which is not always easy to implement with already established production. Also, too rapid quenching may leave residual stresses within the material and even deform the profile. Air-cooled profiles will result in a lower supersaturation of Mg_2Si , but considering thin-walled profiles the cooling rate may suffice in order to reach enough supersaturation whilst avoiding undesired precipitations [16].

After cooling, the profiles may be stretched to lower internal stresses which is especially necessary after water quenching as reductions of 20% to 40% of the

residual stress have been measured [16]. Additionally, this may to a low degree harden the material through strain hardening. After stretching, the profiles are cut into about 6-7 metres long segments in preparation for ageing [19].

2.2.5 Ageing

The final heat treatment of an aluminium extrusion is ageing, which is a prolonged heat treatment where the material will undergo its final microstructural changes. Specifically, with regard to the 6XXX series, the stages of precipitation are many and complex. Early in the process, solute atoms may cluster to then form GP-zones which in turn will influence the formation of subsequent structures that may be needle-like, rod-like or in the form of laths. Finally, the precipitation of Mg_2Si -particles will occur. Depending on temperature and time during ageing, the amount and size of precipitates will be affected, determining the final mechanical properties of the aluminium alloy. Furthermore, the combination of time and temperature during an ageing cycle that results in the greatest strength is called peak ageing [16]. With regards to ductility and fracture toughness during compression, previous work has shown that an over aged alloy performs better than the same alloy that has been underaged or peak-aged [8], [9]. The reason for this is that the slip associated with deformation in aluminium alloys may be better distributed within the material, preventing grain boundary fractures [8].

2.3 Crash boxes, relevant properties and the testing of them

2.3.1 Crash performance and tensile testing

To determine the crash properties of a crash box, compression tests of specimens can be performed. Generally for compression testing in several studies, relevant properties for crash performance include the number of crack initiations, energy absorption and folding behaviour during compression [3], [9], [8], [10], [11]. The force versus displacement curve from the measurements from the compression test equipment will differ with an initial peak load and then the load will drop and rise for every fold initiation in the specimen. A way to handle that is by taking the average of the curve, not counting the initial peak which will be much higher than the following. That average is called *mean crush force* (further noted MCF) [20].

The assessment of the amount and severity of cracking follows a somewhat subjective and qualitative grading scale which has to be adapted to the actual testing circumstances such as the geometry and thickness of the specimen. The grading scale can also vary, but a European standard widely used scale ranges from 0-20 where 0 means total fragmentation and 20 indicates zero cracking. Some minor cracking does not have to be an issue, but at a certain point, the cracking will start to affect the energy absorption properties negatively [9]. The exact limit of an acceptable level of cracking depends on the order of the car manufacturer [20]. Judgement of the folding behaviour of a specimen may include microscopic studies

of the folding area or crack surfaces and the regularity and evenness of folding throughout the specimen [11], [8].

The tensile properties of a material are often determined by uniaxial tensile tests since the testing circumstances are simple with standardised specimen shapes. However, at the point of maximum strain, instability and necking will occur in all cases of tensile testing of ductile materials, and since the measured properties are based on an adoption of a homogeneous behaviour of the specimen i.e. assuming a constant cross-section area, data points measured after necking have occurred can not be taken into account. In cases where large deformations have to be investigated a compression test should be performed instead [21].

However, it can be noted that ductility i.e. the tensile strain before fracture also known as true fracture strain, can be useful as an indicator of the ability of deformation of the material [22]. The true fracture strain can be estimated after a tensile test has been performed by measuring the minimum cross-sectional area after fracture (S_u) and comparing it with the initial fracture area (S_0) with the following Equation 1 [20]:

$$\varepsilon_f = \ln\left(\frac{S_0}{S_u}\right) \quad \text{Eq. 1}$$

2.3.2 Theory of relevant properties

Plastic strain in metals is determined by the ability of dislocations to move. It is the hindering of this movement through different mechanisms that hardens the material and lowers the ductility. Substitutional or interstitial solutes of alloying elements may increase the yield stress by increasing the lattice friction and thus the energy needed for dislocations to move [21]. The amount of alloying elements in aluminium is in most cases very low [17], but it has an impact by means of solute atoms and precipitates of other phases, as mentioned above in 2.1 and 2.2.

The impact of the particles depends on the size and coherency. The strength of the interface between particles and the material depends partly on the coherency. During tensile stress, when the coherency strength is exceeded, voids start to form around the particles. The voids grow quickly and eventually form a micro crack in the middle, turning the specimen into a thin-walled tube before the final fracture. This yields a so-called cup and cone fracture [21].

2.3.3 Previous studies

Reports and investigations connected to the aims of this project were studied and taken into account for the planning of the experimental portion of the project and the drawing of conclusions. J. Mendoza did an internal investigation at SAPA

Technology (nowadays Hydro Extrusion Innovation & Technology) in 2014 in the form of a literature study with a review of a broad range of reports that included the connections between microstructures, crash performance, tensile properties and crash properties of aluminium crash boxes. Most of the studies mentioned in this report are fetched from the references of Mendoza's paper [3].

K. Morita et al. investigated the crash performance and tensile properties with connection to the grain structure and under ageing versus over ageing by calculations of the stress concentrations in the grain boundaries, where it was found that smaller grains decreased the stress concentrations and therefore the risk of crack initiation. Cracking behaviour during compression was better for over ageing and smaller grains [8]. M. Rosefort et al. got similar results with respect to grain size when inspecting folding behaviour on a compression-tested EN AW 6060 profile i.e. that smaller grains improved the folding behaviour [11]. Vazdirvanidis et al. studied folding behaviour and tensile properties on 6063-alloy samples with different ageing cycles from natural ageing up to stable conditions to artificial ageing. They also studied the difference between water and air cooling after extrusion. The water-quenched gave better results for crash performance than the air-cooled which showed grain boundary precipitation on Mg_2Si . Tensile tests were also performed [10].

In the article written by Parson et al., they have included some alloys from both the soft (including 6063) and medium strength 6XXX alloy categories aged at different times and temperatures from under to over aged including peak-aged. Crash performance was investigated through a compression test with the calculation of MCF and crack rating. Tensile tests were also performed. Also here, it was clear that fracture strain was improved by over ageing for all alloys and that higher cooling rates during quenching gave less grain boundary precipitation and thus higher grain boundary strength; resulting in greater ductility for a set strength for water quenched samples. All soft alloy samples were fully recrystallised to a fine grain structure. Parson et al. also investigated if there might be any correlations between tensile test parameters and crash performance parameters which could be seen in some cases. The most interesting results for this project were that ultimate tensile strength and MCF had a linear relationship for a wide range of the specimens and that the true fracture strain for soft alloys, regarding the specific profile, seemed to have a critical lower value at 0,7 where the crack grading quite abruptly went from one or more cracks to no cracks for both air and water-quenched extrusions [9].

With the aim to further investigate correlations in mechanical testing, an internal investigation by A. Assisi was performed at Hydro Extrusion Sweden AB in 2021. The investigation used samples from extruded crash box models which were treated with different ageing cycles. It is possible to see some trends in the stress-strain curves with increasing ageing time; an increasing difference between the ultimate tensile strength (here noted R_m) and the last point recorded in the tensile test, here

noted R_f , or “fracture stress”, was observed [14]. Note that what is interesting is how large the recorded difference is, and not that R_f is to be regarded as the actual fracture stress in the specimen since that type of conclusion should not be drawn from a tensile test data point after necking occurred [21].

Tensile tests were performed and different parameters were plotted against each other. The area reduction (further noted Z) was measured with the help of a stereo microscope. Since true fracture strain can be derived from Z , it was considered as a parameter of ductility (true fracture strain can be seen as a pretty good predictor of ductility as motivated in other sources [20], [22]). It was found that yield strength and the area reduction during necking had a strong correlation with increasing ageing time which is as expected, as though yield strength decreases with increasing ductility. It was also found that the difference between R_m and R_f had a similar and nearly as strong relation to decreasing yield strength as area reduction which indicates that $R_m - R_f$ could be a possible parameter of ductility as well. In extension, area reduction and $R_m - R_f$ were also plotted against each other which showed their strong relationship. These results may be combined with the results from studies by Parson et al. [15] (cited in the internal investigation. This unpublished study by Parson et al. is partly the same as the published article referred to above) since true fracture strain can be derived from the area reduction. However, to be able to draw accurate connections between tensile test parameters and crash performance parameters these types of correlations have to be more widely investigated [14].

Assisi also emphasises that larger data sets are needed to be more certain about the found relationship between area reduction and $R_m - R_f$. Furthermore, Assisi has only considered water-quenched extrusions in the report [14]. In this study, the found relationships of the internal investigation will be examined for both water- and air-quenched aluminium extrusions of a crash box model. Furthermore, possible connections between the tensile test parameters and compression test parameters will be examined in a similar manner as in the studies by Parson et al. [9], [15].

3. Method

Extrusion, ageing programs and all measurements were performed at Hydro Extrusion Sweden AB in Finspång. For all the test iterations, three samples for every ageing program and cooling rate were tested and mean values were calculated.

3.1 Extrusion, quenching and ageing

The alloy that is used in this project is within the EN AW 6063 range, but there are always differences in the exact chemical composition. The more precise composition of the material that was actually used can be found in Table 1. Five cylindrical billets with a diameter of 317 mm were extruded through a crash box profile tool in an extrusion press at Hydro Extrusions in Finspång. The billets were heated up to 485 °C before extrusion, then they had an outlet temperature of about 550 °C directly after extrusion and had a profile run out speed of 13 m/min. Billet no. 1 was a startup billet whose purpose was for the extruder to reach proper operating conditions with regards to for example temperature and run out speed.

Consequently, profile no. 1 was discarded after extrusion. Profiles from billets no. 2 and 3 i.e. profiles no. 2 and 3 were water-quenched after extrusion and profiles no. 4 and 5 were air-cooled after extrusion. The cooling rate was measured by a fork thermocouple placed on top of the profile at the outlet of the press, letting it pass by the quench box. Every billet resulted in an extrusion of about 40 metres. The profiles were stretched out about 0.2-0.3 % of their length and then lengths of 3500 mm and 2500 mm were cut off at the front and the end of the profiles respectively. Samples with lengths of around 300 mm were sawn out from the profiles and carefully marked. The profile cross-section can be seen in Figure 2.

Tab. 1 The specific chemical composition of the alloy used in this experiment.

Alloying element	Si	Fe	Cu	Mn	Mg	Cr	Ni
Content [wt%]	0.52	0.19	0.01	0.05	0.47	<0.01	0.01
Alloying element	Zn	Ti	Pb	Ca	Zr	V	Al
Content [wt%]	0.02	0.01	<0.01	<0.01	<0.01	0.01	98.68

To be able to investigate the impact of ageing on the results, different ageing programs from under to over aged were performed in lab furnaces. For the under aged samples, two programmes were performed; 165 °C for 3 and 6 hours. One program for peak-ageing was performed at 180 °C for 5 hours and 40 minutes. Finally, for the over aged samples, a temperature of 215 °C was used in combination with four different times; 1, 2, 4 and 6 hours. Both water and air-quenched samples were used in all ageing programs. As-extruded i.e. unaged samples (further noted T4), both water and air-quenched, were picked out as references.

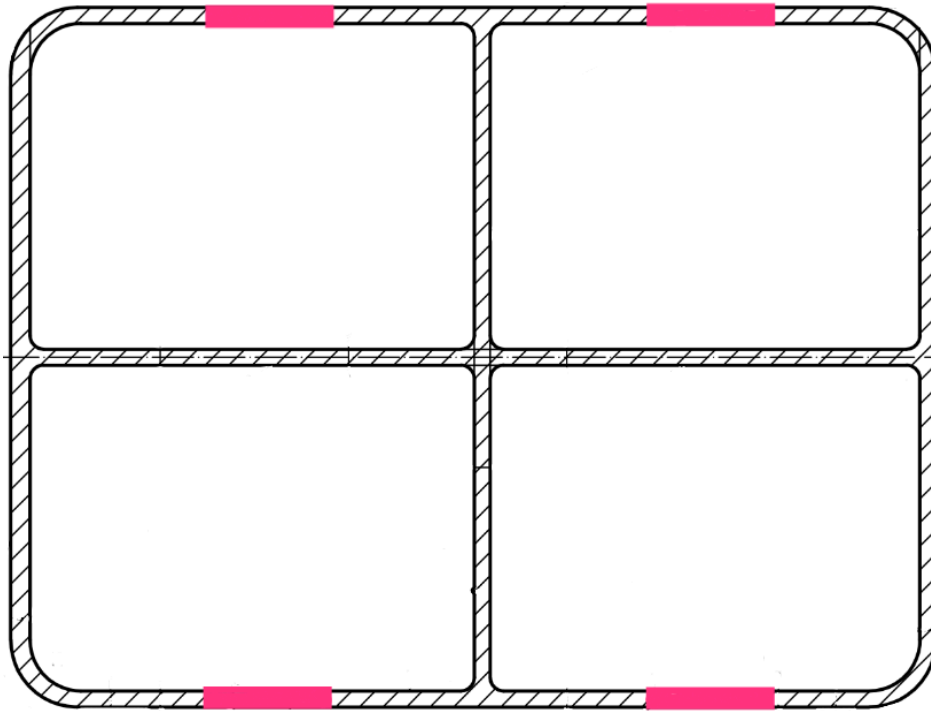


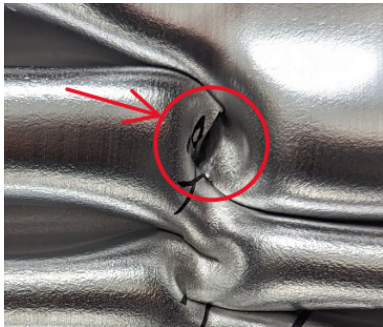




Fig. 2 The cross-section of the profile extruded in the study. The red areas represent the approximate places where tensile test samples were extracted.

3.2 Compression test

Compression tests were performed by compressing crash boxes in the extrusion direction. The profile sample lengths were reduced from around 300 to 120 mm by a compression speed of 100 mm/min. Crash force against deformation was recorded and mean crush force (MCF) was automatically calculated. Compressed samples were visually inspected and photographed to then be judged from a degree of cracking using a standard formulated together with Hydro Extrusion Sweden AB in Table 2.

Tab. 2 Quantification of the degree of cracking of crash boxes.

Grade	Explanation	Image example
1	No cracking	
2	Surface cracking, no penetration	
3	Cracking through the entire thickness in T-joints of the profile.	
4	Cracking through the entire thickness of outside folds. Alternatively, a high degree of waviness and cracking on folds	
5	Large cracks over 25 [mm] or complete fragmentation	

3.3 Tensile test

The three tensile test samples from every cooling rate and ageing cycle including T4 were sawn and milled from the long side outside wall of a piece of profile (see Figure 2). The samples were dogbone-shaped according to standard ISO 6892 and in the middle was a crack initiation. The exact cross-section area of every sample was measured before the test and is designated as S_0 . Stress and strain were recorded for the whole testing course by the testing equipment and the yield strength $R_{p0.2}$ and ultimate tensile strength R_m were specified whereupon R_f was taken out from every test log defined as the last point of stress recorded.

3.4 Area reduction measurements and microscopy

To be able to calculate the area reduction Z , the area of the fracture surface (S_u) was measured under a stereo microscope with the fracture surface up. A picture was taken (see Figures 6 through 13) whereupon a drawing tool was used to approximately mark the fracture surface outlines. A computer program calculated the marked fracture surface area which was then written down. Both fracture surfaces from every tensile test sample were measured. It should be noted that since the photos were taken from above, the measured area equalises the flat horizontal projection of the fracture surface.

Further, microscopic pictures were taken of the fractures from some of the samples from the side to study the eventual visual difference between the water and air-quenched material. For this, the deformed part of the samples was sawn out and mounted into bakelite. Then these samples were ground with SiC paper of size P220 to P200, then diamond-polished with 9, 3 and 1 microns and finally polished with a 10% SiO 90% ethanol mixture and then another time with ethanol only. Over aged 215 °C in 6 hours and peak-aged at 180 °C 5 hours and 40 minutes, both water and air-quenched were studied.

Then microscope photos were taken of the grains to investigate eventual visual differences between extrusion directions and between water and air-quenched material in the microstructure. For this, smaller samples from the undeformed parts of the tensile test samples were sawn out. Surfaces both in the extrusion direction and against were grinded and polished in the same manner as described above, however, they were not mounted. The last step of this sample preparation was anodising the surface in HF with a platinum net. Microscope photos were taken with a filter that revealed crystallographic direction by different colours on the grains. Peak-aged samples were studied in this step.

3.5 Implementation of calculations and plots

For every combination of cooling methods and ageing cycles, the mean value of the three samples was calculated. The following Equation 2 was used to calculate the area reduction Z for every sample:

$$Z = \frac{S_0 - S_u}{S_0} \cdot 100 \text{ [\%]} \quad \text{Eq. 2}$$

True fracture strain ε_f was calculated according to Equation 1 and multiplied by 100 to get the percentage. Since both fracture surfaces were measured for every tensile test sample, there are two S_u values connected to every sample ID. For every sample, the mean Z-value was calculated with the mean of the two S_u -values. Then, the conclusive Z-values for every type of cooling and ageing cycle combination were calculated using the three samples measured for each iteration of parameters. The same procedure was done when calculating the mean of ε_f . Microsoft Excel and Google Sheets were interchangeably used to calculate the mean values and to plot the measured parameters against each other to try to find possible correlations and to produce equations and coefficients of determination, i.e., R^2 values. Standard deviations were also calculated for all the mean values and shallowly analysed.

4. Results

In this chapter of the report, experimental values regarding compression- and tensile testing are presented and compared, building upon work already done by A. Assisi [14] and N. Parson et al. [9]. Additionally, the measured cooling rate of extrusions as well as microstructural observations are presented.

4.1 Cooling rate of extrusions

In Figure 3, the cooling rate of the four extrusions are presented. Every billet exiting the die holds an initial temperature of approximately 530 °C. The extrusions subsequent to billet 2 and 3 are water-quenched whilst the extrusions subsequent to billet 4 and 5 are air-cooled. The average cooling rates between the initial temperature and 250 °C and the maximal cooling rates are presented in Table 3.

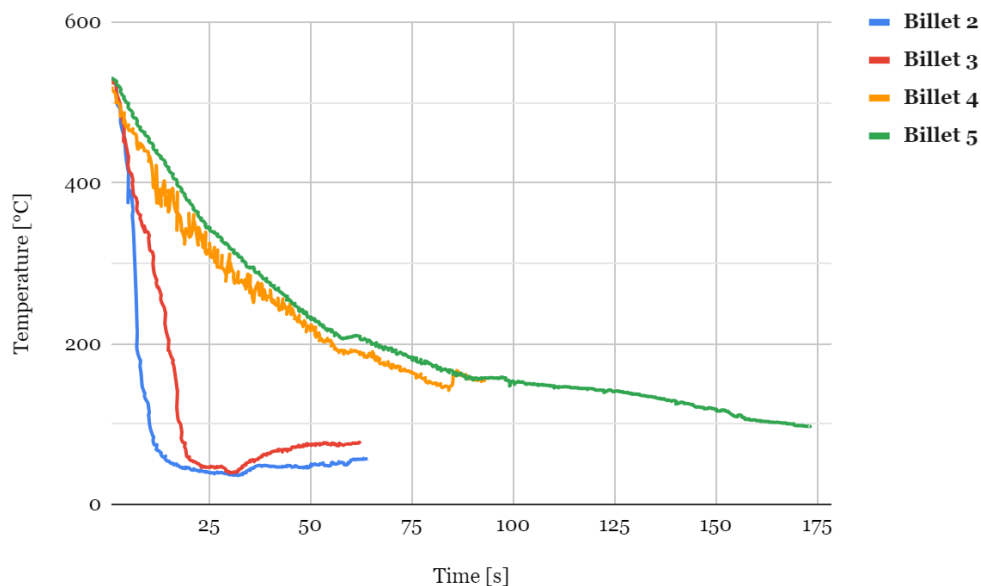


Fig 3. The cooling rate of four extrusions. Billets 2 and 3 are water-quenched whilst billets 4 and 5 are air-cooled.

Tab. 3 Cooling rates of the billets

Billet	Type of cooling	Average cooling rate [°C/s]
2	Water	45.9
3	Water	21.7
4	Air	6.62
5	Air	6.18

4.2 Tensile test

Figures 4 and 5 display a collection of tensile testing curves following different cooling rates and ageing cycles. Please note that each curve represents the first tensile test out of three performed and that the ledger specifies both the ageing cycle and cooling medium where T4 represents an alloy tested as extruded.

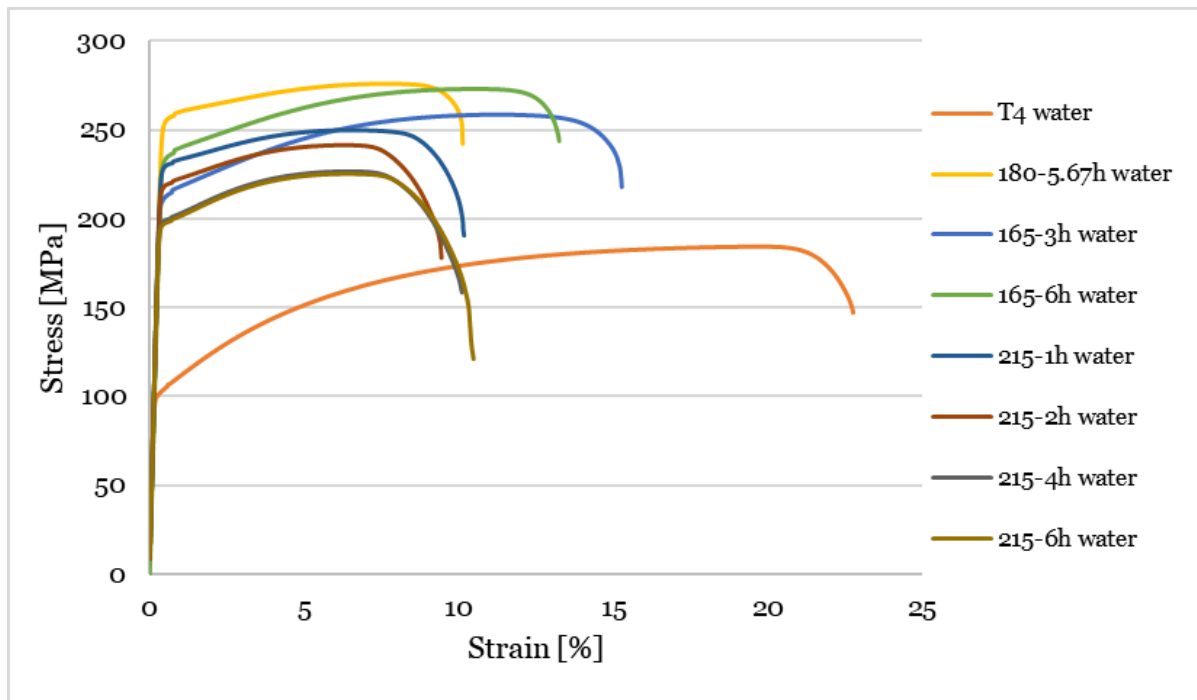


Fig. 4 Tensile tests of water-quenched samples. Each curve represents the first of three tests performed with the exception of “215-4h water” which is represented by the second test performed as the first had outlier values.

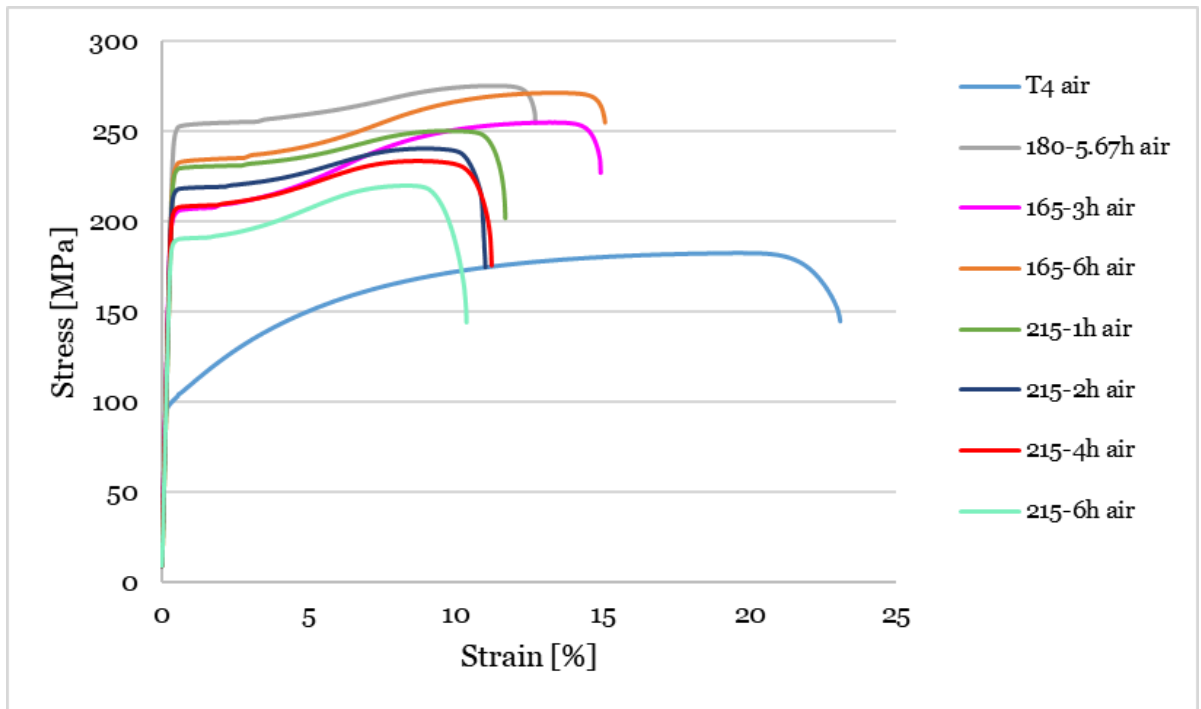


Fig. 5 Tensile tests of air-cooled samples

The following Figures 6 through 13 are a selection of the images of the fracture surfaces of tensile test samples where the lighter grey areas in the images are the fracture areas. All other images are to be found in Appendix B. Furthermore, a collection of relevant mean values surrounding the tensile testing is presented in Tables 4 and 5. The mean values are drawn from 3 samples however with one exception: one abnormal value was recorded for the R_f value for one of the samples of 215 °C, 4h ageing, so for the R_f value, this sample's result was counted away. This is further discussed in 5.1.1.

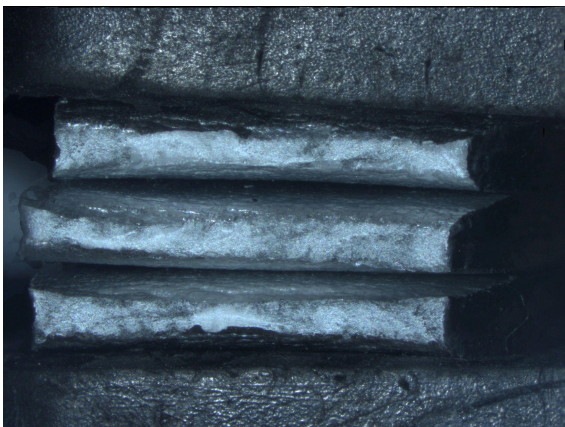


Fig. 6, T4 water-quenched.



Fig. 7, T4 - air-cooled.

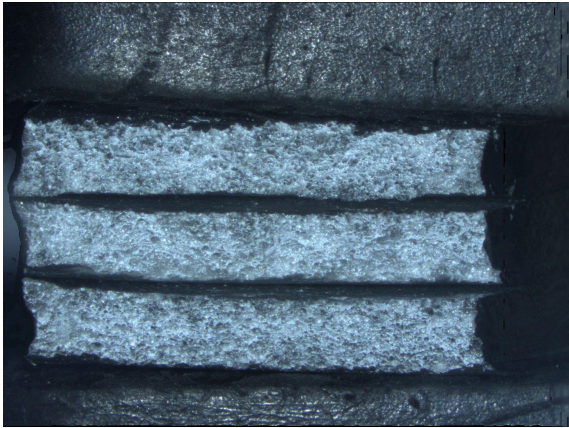


Fig. 8 Peak-aged, water-quenched.

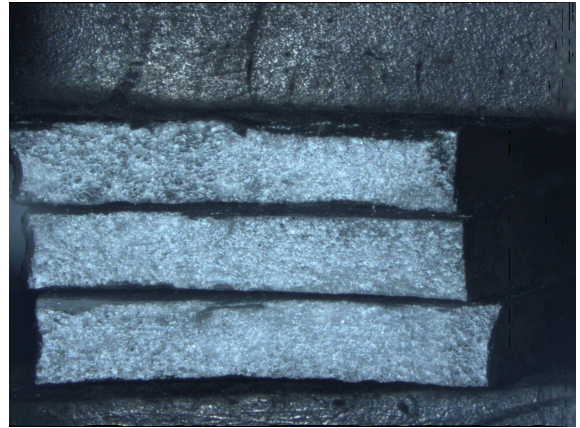


Fig. 9 Peak-aged, air-cooled.

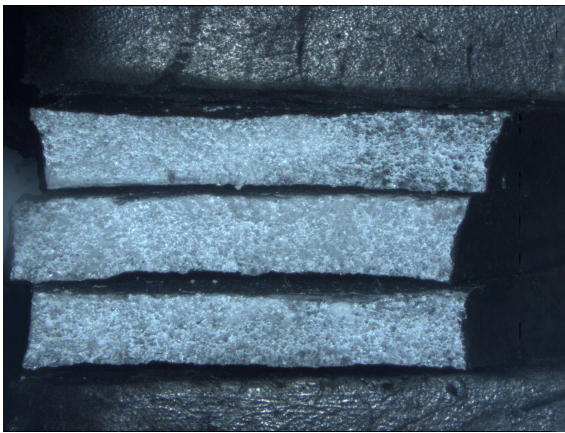


Fig. 10 165/3h water-quenched.

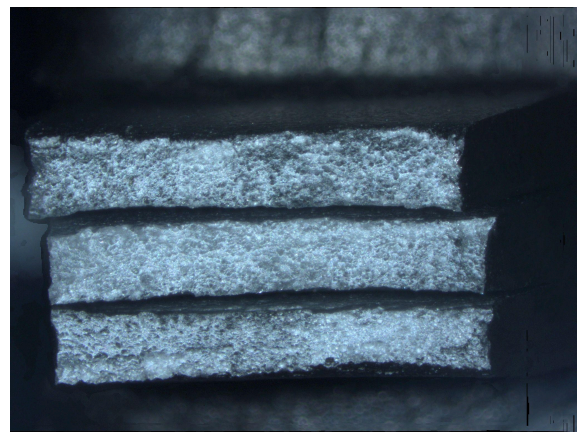


Fig. 11 165/3h air-cooled.

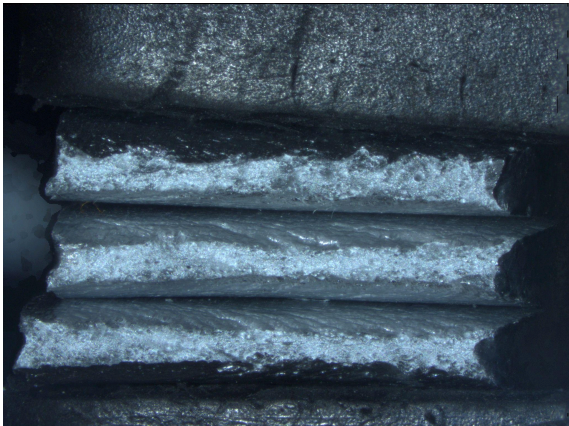


Fig. 12 215/6h water-quenched.



Fig. 13 215/6h air-cooled.

Tab. 4 Gathered tensile test results for water-quenched samples (mean values with standard deviation). Please note that Mean R_m - R_f for 215°C/4h is calculated with two values as one measurement of R_f was abnormally low.

Sample description	Mean R_m [MPa]	Mean $R_{p0.2}$ [MPa]	Mean Z [%]	Mean true fracture strain [%]	Mean R_m - R_f [Mpa]	Mean S_o [mm ²]	Mean S_u [mm ²]	No. samples
T4	185 ± 1.01	102 ± 1.09	68.0 ± 2.11	114 ± 6.67	49.0 ± 12.6	28.8 ± 0.644	9.21 ± 0.406	3
165°C/3h	259 ± 1.81	213 ± 3.38	39.2 ± 1.51	49.7 ± 2.49	45.2 ± 5.33	29.2 ± 0.775	17.7 ± 0.359	3
165°C/6h	274 ± 1.09	237 ± 1.90	33.3 ± 3.97	40.7 ± 6.03	29.1 ± 7.10	29.2 ± 0.678	19.5 ± 1.59	3
180°C/5.67h	277 ± 1.57	258 ± 1.58	31.0 ± 1.41	37.1 ± 2.03	32.9 ± 0.882	29.3 ± 0.461	20.2 ± 0.151	3
215°C/1h	248 ± 1.78	228 ± 1.69	46.9 ± 3.60	63.4 ± 6.91	59.8 ± 15.0	29.6 ± 0.187	15.7 ± 1.13	3
215°C/2h	239 ± 1.82	217 ± 1.45	51.1 ± 2.18	71.7 ± 4.52	76.3 ± 14.1	29.6 ± 0.255	14.4 ± 0.524	3
215°C/4h	227 ± 0.366	199 ± 0.317	66.7 ± 0.468	110 ± 1.01	75.8 ± 11.0	29.1 ± 0.852	9.72 ± 0.192	3 (2 for R_f)
215°C/6h	225 ± 1.24	197 ± 1.54	66.4 ± 2.89	109 ± 8.63	100 ± 12.8	29.2 ± 0.537	9.82 ± 0.846	3

Tab. 5 Gathered tensile test results for air-cooled samples (mean values with standard deviation).

Sample description	Mean R_m [MPa]	Mean $R_{p0.2}$ [MPa]	Mean Z [%]	Mean true fracture strain [%]	Mean R_m - R_f [Mpa]	Mean S_o [mm ²]	Mean S_u [mm ²]	No. samples
T4	183 ± 0.304	100 ± 0.626	59.7 ± 2.90	91.2 ± 7.26	53.2 ± 22.3	29.2 ± 0.343	11.8 ± 0.948	3
165°C/3h	254 ± 0.657	204 ± 0.956	34.9 ± 5.20	43.1 ± 8.18	31.3 ± 3.13	29.2 ± 0.259	19.0 ± 1.67	3
165°C/6h	271 ± 0.434	233 ± 0.585	28.9 ± 2.48	34.2 ± 3.46	21.5 ± 4.62	29.0 ± 0.448	20.6 ± 0.770	3
180°C/5.67h	276 ± 1.31	254 ± 1.00	29.3 ± 1.55	34.7 ± 2.18	20.5 ± 0.446	29.2 ± 0.248	20.6 ± 0.306	3
215°C/1h	249 ± 1.23	228 ± 1.20	35.0 ± 2.04	43.2 ± 3.13	40.7 ± 6.80	29.3 ± 0.164	19.1 ± 0.498	3
215°C/2h	239 ± 1.72	216 ± 1.73	43.0 ± 3.11	56.2 ± 5.51	68.1 ± 9.91	29.3 ± 0.173	16.7 ± 1.00	3
215°C/4h	232 ± 1.16	205 ± 1.59	45.4 ± 3.58	60.6 ± 6.64	62.1 ± 8.06	29.1 ± 0.650	15.9 ± 1.37	3
215°C/6h	220 ± 0.23	189 ± 0.158	58.9 ± 2.46	89.1 ± 5.92	85.1 ± 17.3	29.1 ± 0.626	11.9 ± 0.887	3

4.3 Compression test

Following compression tests, Figure 14 displays the different gradings crash boxes received according to the grading scale explained in section 3.2. Furthermore, results from the compression tests are presented in Tables 6 and 7. Figure 15 represents the relation between MCF and strength parameters from the tensile tests.

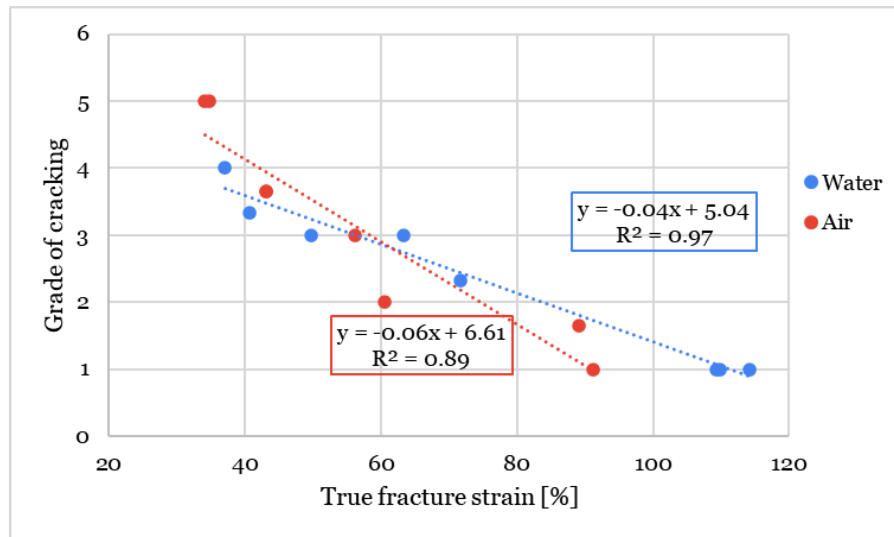


Fig. 14 Grade of cracking with respect to true fracture strain. Including all aged and unaged samples.

Tab. 6 Gathered compression test results for water-quenched samples (mean values with standard deviation).

Sample description	Mean MCF [kN]	Grade of cracking
T4	104 ± 0.98	1 ± 0.00
165°C/3h	163 ± 2.19	3 ± 0.00
165°C/6h	173 ± 2.19	3.33 ± 0.00
180°C/5,67h	175 ± 0.88	4 ± 0.00
215°C/1h	166 ± 5.65	3 ± 0.00
215°C/2h	159 ± 1.28	2.33 ± 1.15
215°C/4h	147 ± 3.45	1 ± 0.00
215°C/6h	139 ± 0.79	1 ± 0.00

Tab. 7 Gathered compression test results for air-cooled samples (mean values with standard deviation).

Sample description	Mean MCF [kN]	Grade of cracking
T4	103 ± 1.52	1 ± 0.00
165°C/3h	159 ± 0.62	3.66 ± 0.58
165°C/6h	170 ± 2.40	5 ± 0.00
180°C/5,67h	165 ± 6.61	5 ± 0.00
215°C/1h	163 ± 4.18	3.66 ± 0.58
215°C/2h	159 ± 1.75	3 ± 0.00
215°C/4h	150 ± 2.12	2 ± 1.00
215°C/6h	141 ± 4.05	1.66 ± 1.15

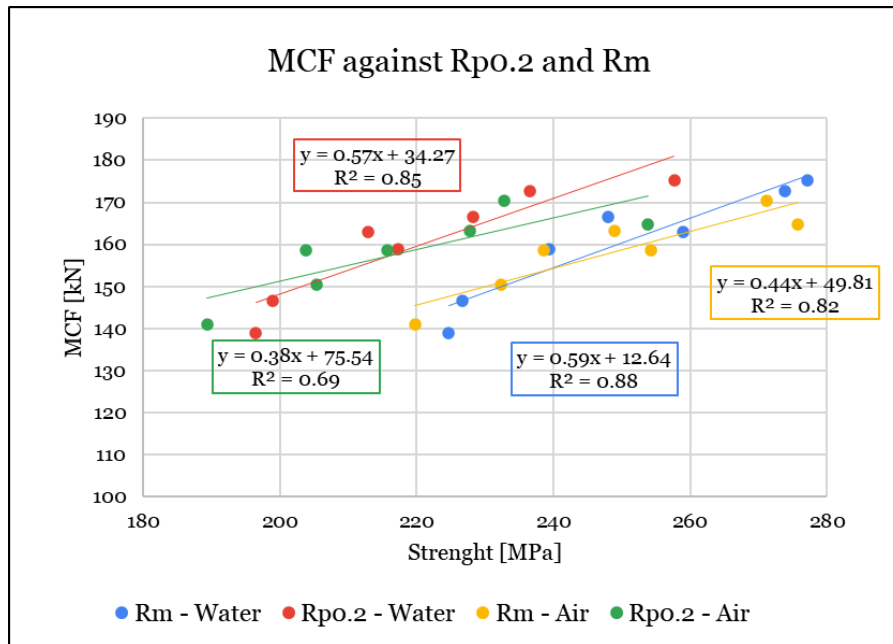


Fig. 15 MCF versus the strength of all samples. Divided with respect to cooling methods and strength parameters.

4.4 Evaluation of ductility parameters

The following Figures 16 through 18 are used in order to evaluate parameters' inherent ability to represent the correlation between strength and ductility depending on the ageing time of an over aged aluminium alloy. Furthermore, Figures 19 a) through 24 b) are plots exposing the correlation between strength and ductility depending on ageing time and method of cooling. Finally, Figure 25 displays the correlation between R_m - R_f and the area reduction Z .

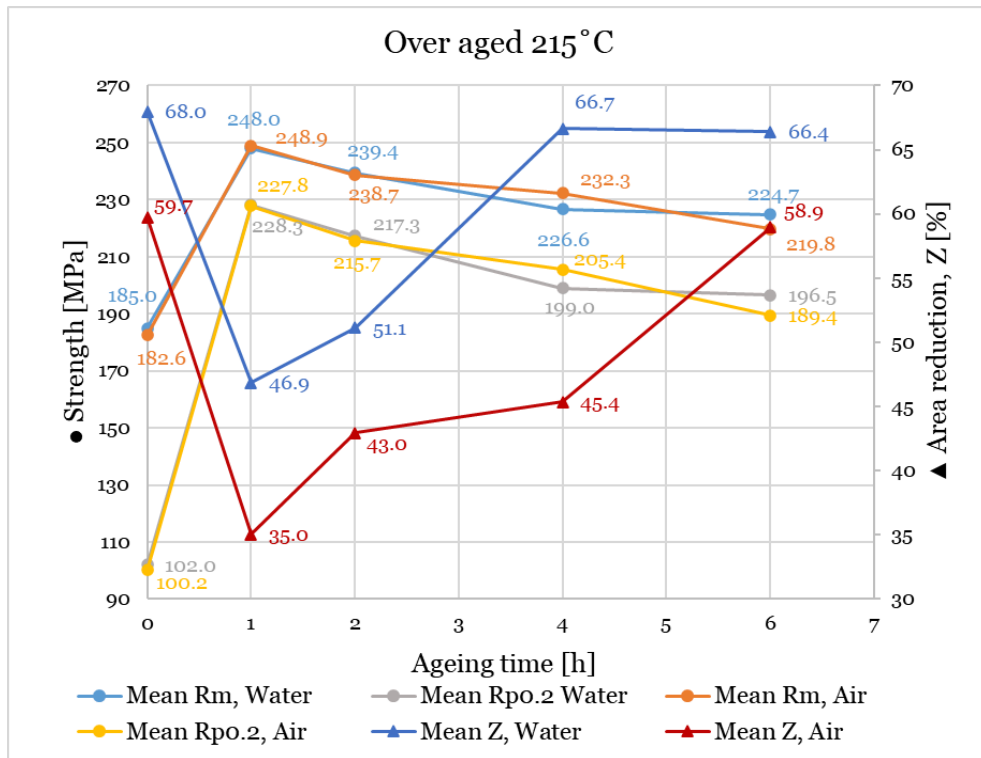


Fig. 16 Water- and air-quenched samples' relation between R_m and area reduction, Z . The samples have been over aged at 215°C for different lengths of time where 0 hours means T_4 .

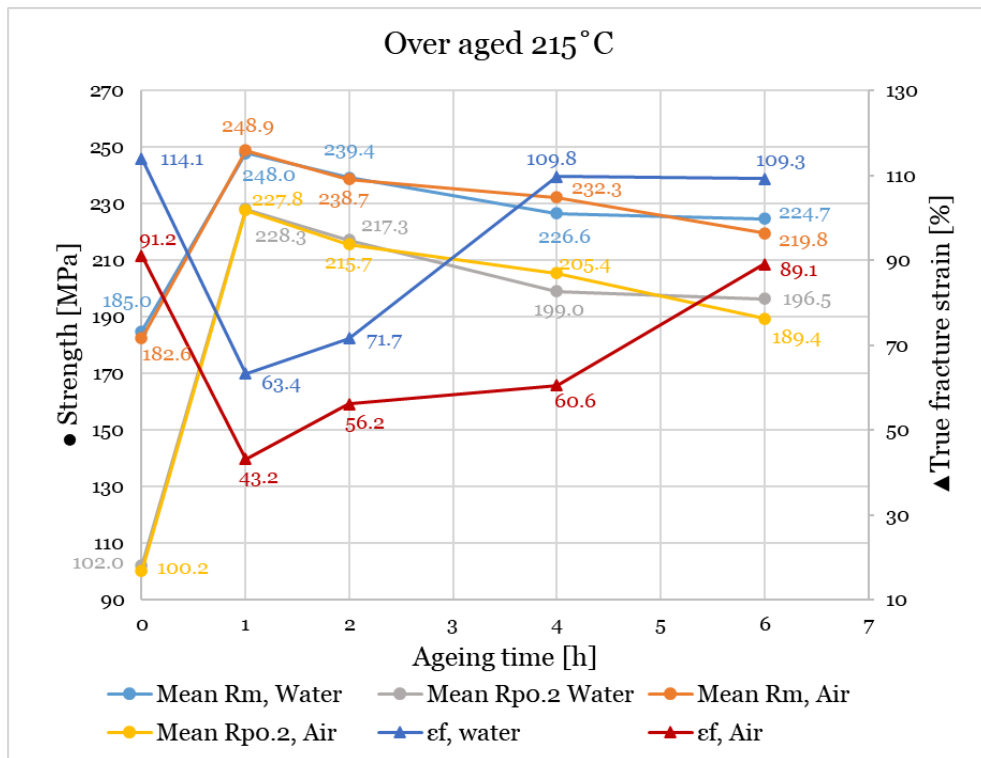


Fig. 17 Water- and air-quenched samples' relation between R_m and true fracture strain, ϵ_f . The samples have been over aged at 215°C for different lengths of time where 0 hours means T_4 .

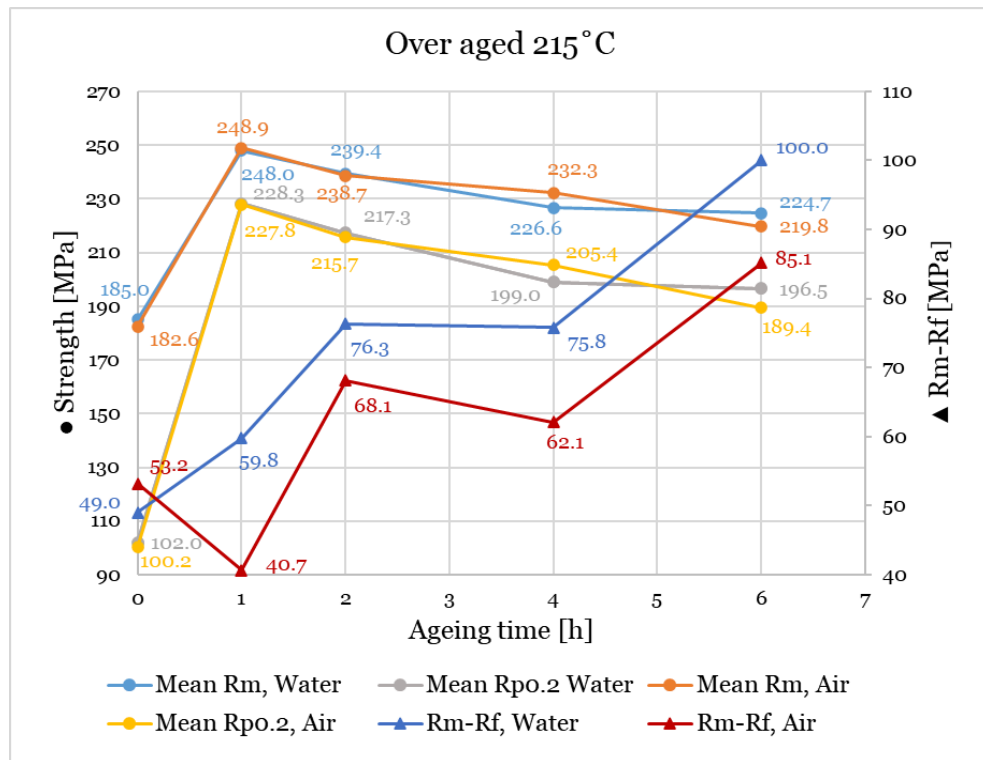


Fig. 18 Water- and air-quenched samples' relation between $R_{po.2}$, R_m and R_m-R_f . The samples have been over aged at 215°C for different lengths of time where 0 hours means T4. Please note that the R_m-R_f value corresponding to the water-quenched samples aged in 4 h is evaluated from two tests due to an outlier value.

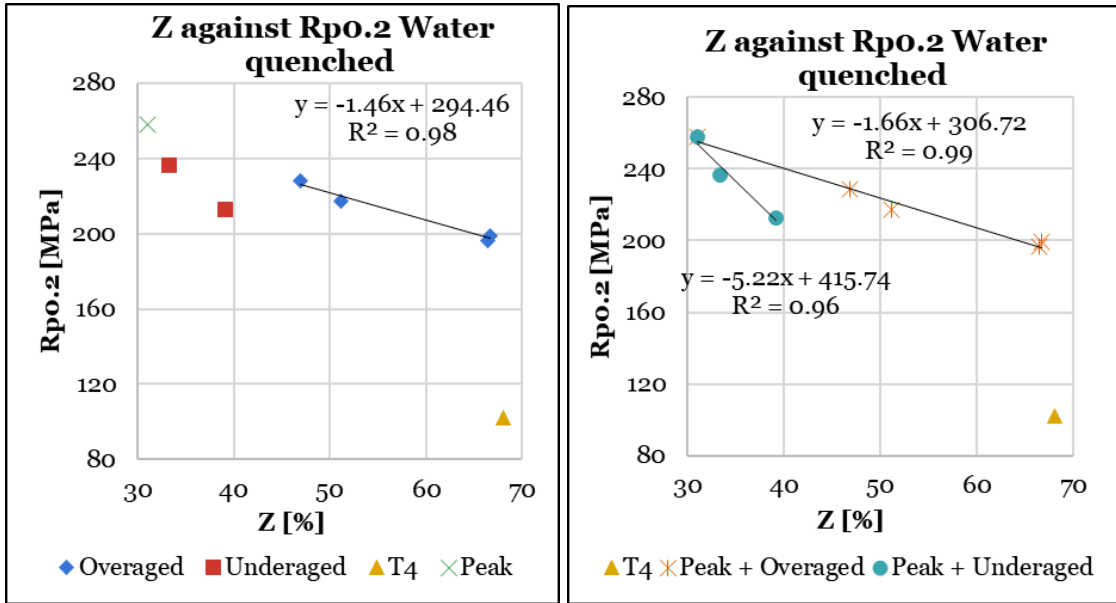


Fig. 19 a) and b), Z versus $R_{p0.2}$ for water-quenched samples. In Fig. 19 a) the ductility correlation of solely over aged samples is displayed while Fig. 19 b) displays the correlation of over aged samples and underaged samples in conjunction with peak-aged samples.

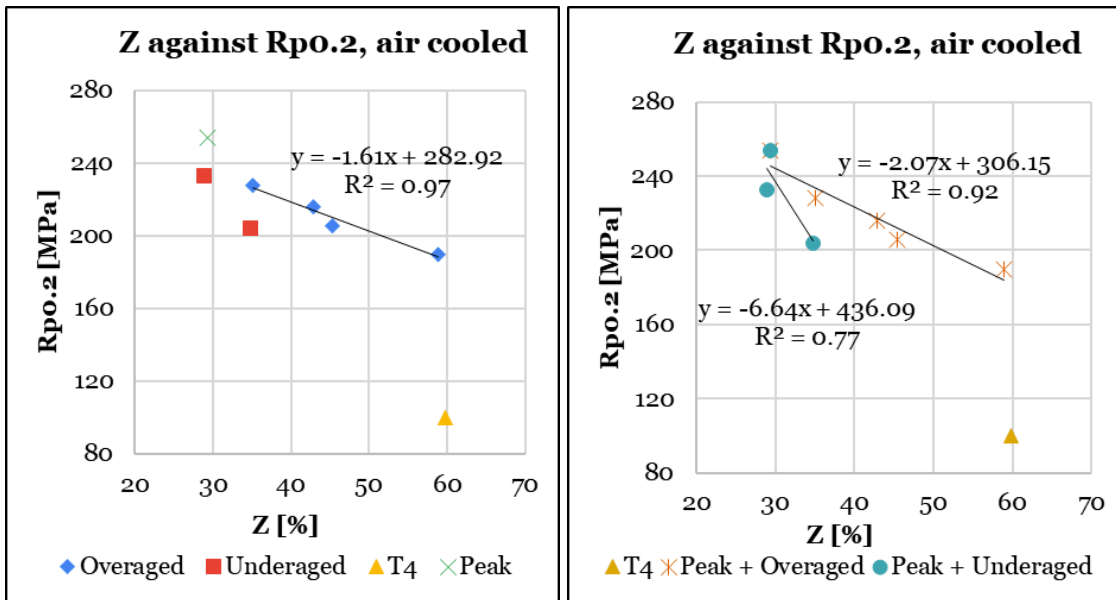


Fig. 20 a) and b), Z versus $R_{p0.2}$ for air-cooled samples. In Fig. 20 a) the ductility correlation of solely over aged samples is displayed while Fig. 20 b) displays the correlation of over aged samples and underaged samples in conjunction with peak-aged samples.

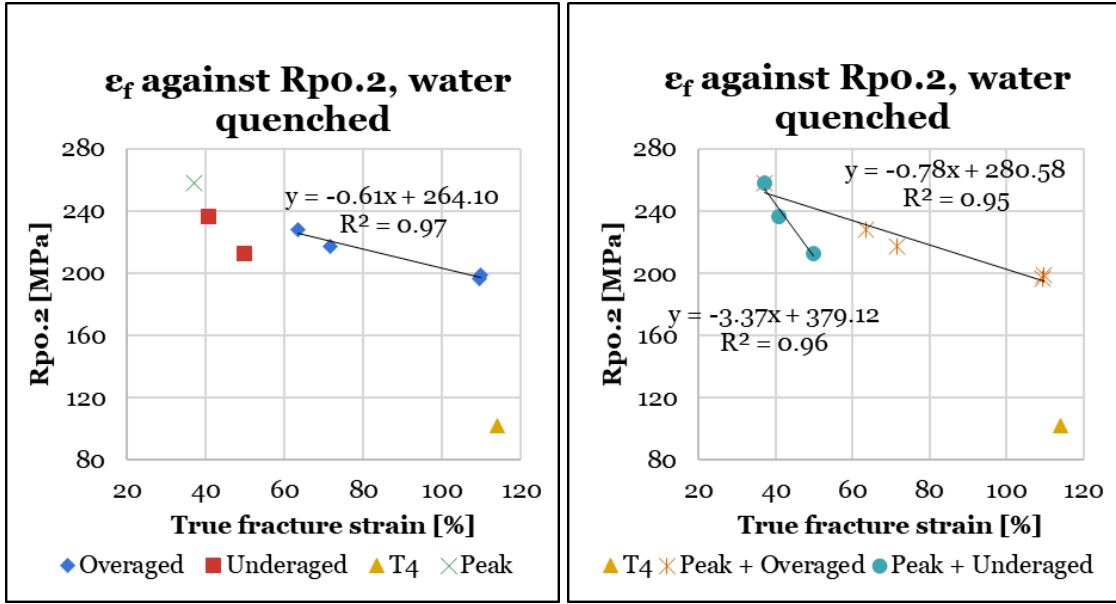


Fig. 21 a) and b), ϵ_f versus $R_{p0.2}$ for water-quenched samples. In Fig. 21 a) the ductility correlation of solely over aged samples is displayed while Fig. 21 b) displays the correlation of over aged samples and underaged samples in conjunction with peak-aged samples.

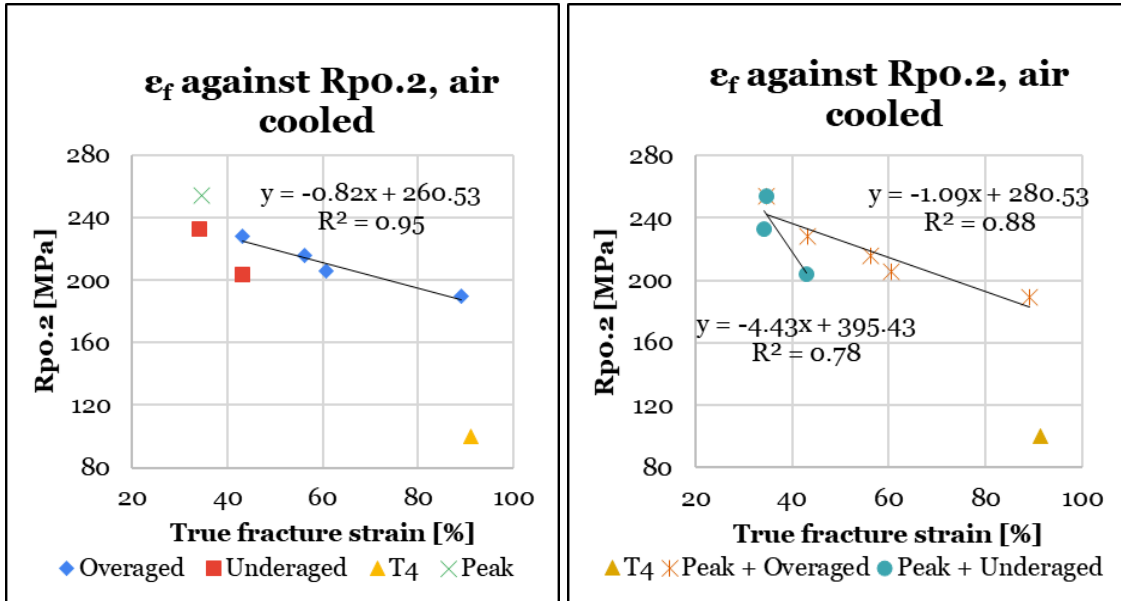


Fig. 22 a) and b), ϵ_f versus $R_{p0.2}$ for air-cooled samples. In Fig. 22 a) the ductility correlation of solely over aged samples is displayed while Fig. 22 b) displays the correlation of over aged samples and underaged samples in conjunction with peak-aged samples.

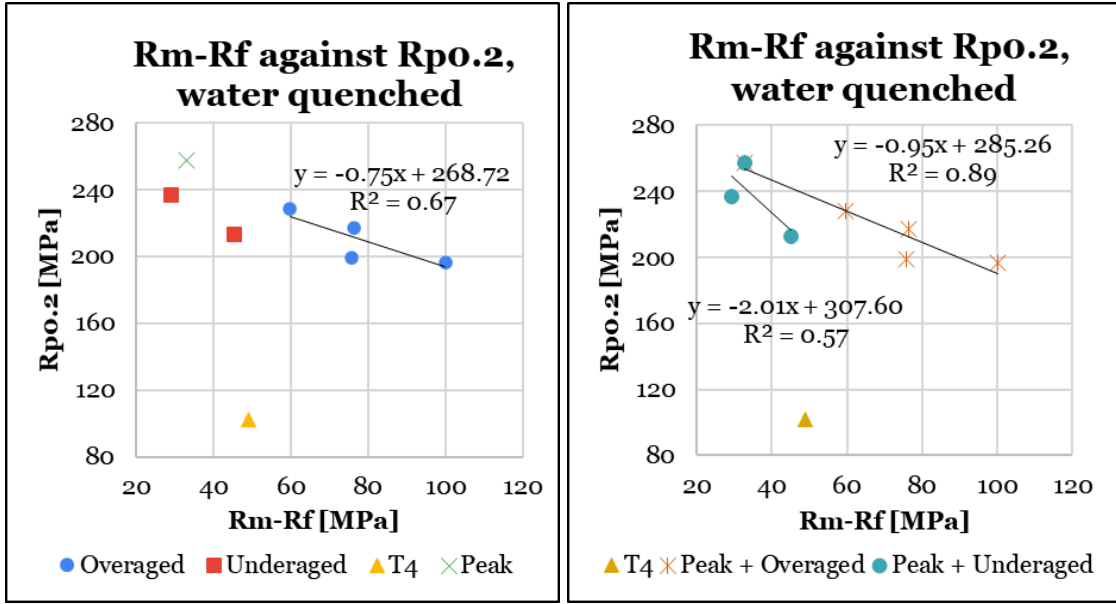


Fig. 23 a) and b), $R_m - R_f$ versus $R_{po.2}$ for water-quenched samples. In Fig. 23 a) the ductility correlation of solely over aged samples is displayed while Fig. 23 b) displays the correlation of over aged samples and underaged samples in conjunction with peak-aged samples. Please note that the $R_m - R_f$ value corresponding to the samples aged in 4 h is evaluated from two tests due to an outlier value.

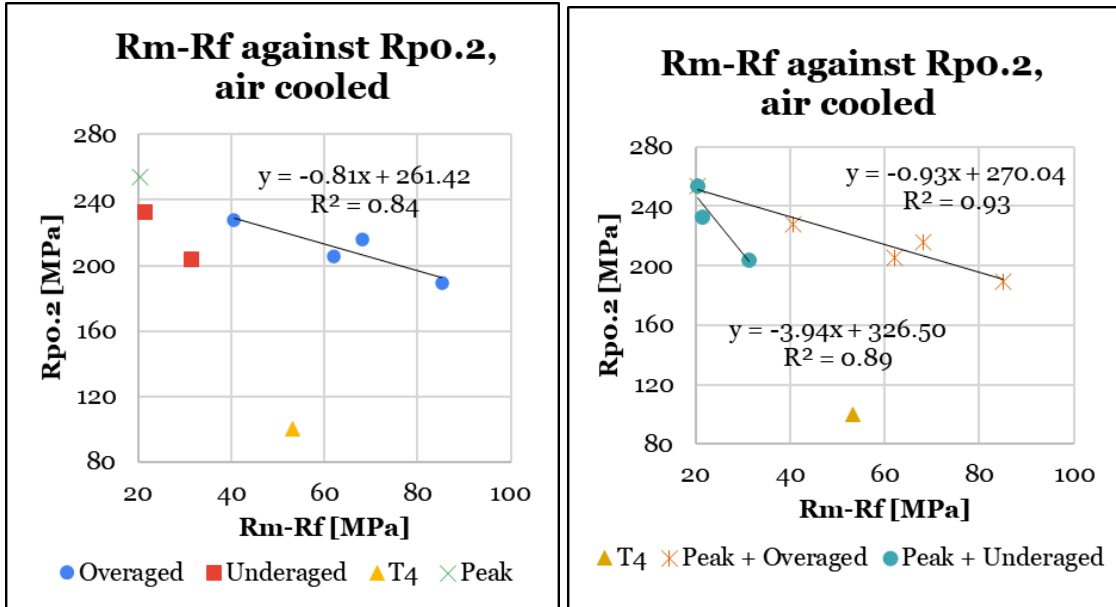


Fig. 24 a) and b), $R_m - R_f$ versus $R_{po.2}$ for air-cooled samples. In Fig. 24 a) the ductility correlation of solely over aged samples is displayed while Fig. 24 b) displays the correlation of over aged samples and underaged samples in conjunction with peak-aged samples.

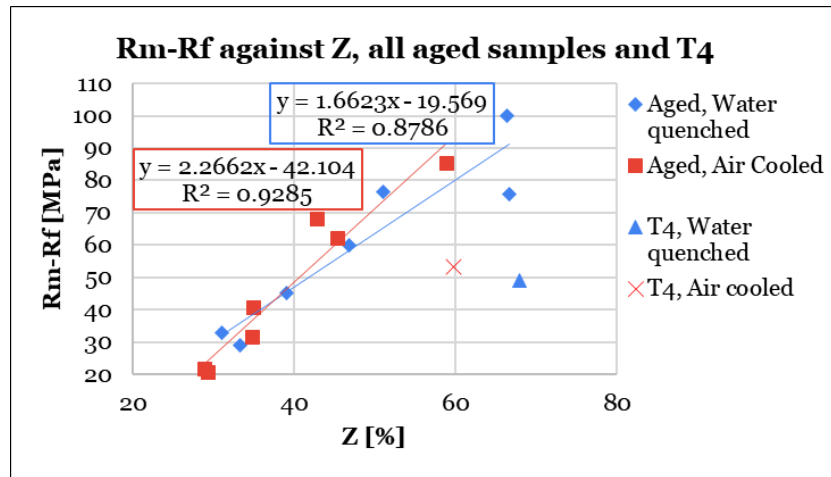


Fig. 25 R_m-R_f versus Z for all aged samples with both cooling methods displayed with their respective correlation. Both T4 values are included as well, however not in the formulas as they are not relevant.

4.5 Microstructural observations

Pictures of the fracture surfaces of tensile test samples that have been water- or air-quenched and aged for 6 h at 215°C are presented here in Figures 26 and 27 respectively. The other pictures taken with the stereo microscope are located in Appendix B. Please note that only pictures of samples that were peak-aged and over aged for 6 h were taken due to the limited time available to prepare the samples. Moreover, in Appendix B, there are also pictures of the microstructure of peak-aged samples, both water- and air-quenched, taken parallel to and perpendicular to the extrusion direction.

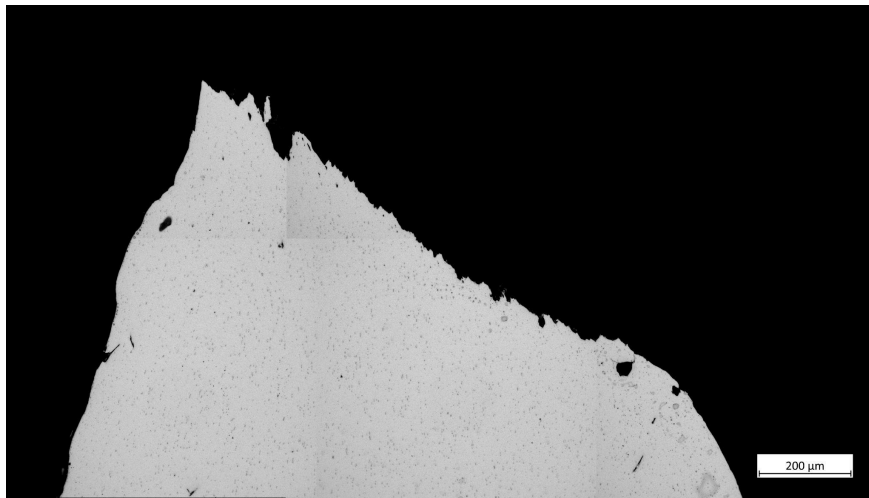


Fig. 26 The fracture surface of the tensile test sample that has been water-quenched and aged for 6h at 215°C.

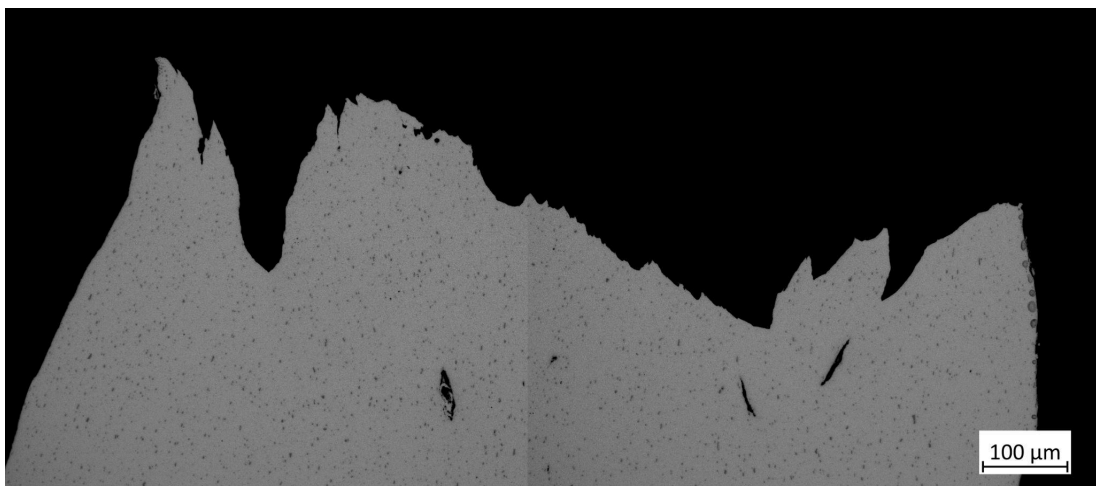


Fig. 27 The fracture surface of the tensile test sample that has been air-cooled and aged for 6h at 215°C.

5. Discussion

5.1 Evaluation of results

5.1.1 Tensile test results

A comment on the difference in shape of the tensile curves between the water-quenched and air-cooled samples, seen in figures 4 and 5, is that strain hardening briefly flattens the air-cooled curves out after the yielding point, which creates slightly crooked curves. Following a discussion with our supervisor Oskar Altzar and Andreas Assisi this is not a common behaviour.

The first of the water-quenched samples aged at 215 °C for 4 hours gave a quite extreme deflection with a low R_f value and ended with a slightly crooked curve. What this depends on is unclear but a theory discussed with the supervisors of this project is that some abnormality might have happened during the test where the sample perhaps have slipped due to not being clamped tightly enough. Because of this, only the last two of the samples were taken into account for the mean value of R_f for the actual combination of cooling method and ageing cycle.

The microscope pictures of fracture surfaces after tensile tests tell a difference between water-quenched and air-cooled samples for over aged samples (see Figures 6 through 13 and Appendix B). The over aged and water-quenched samples showed a more ductile-looking fracture surface than the over aged and air-cooled which have less necking visible in the aforementioned Figures. This is mirrored in both the area reduction measurements and the degree of cracking with a generally smaller area reduction and a higher degree of cracking for the air-cooled samples. This result was expected with respect to literature and results from previous studies [16], [10], [9].

5.1.2 Grade of Cracking and True Fracture Strain

The method of quantification of the degree of cracking presented in Table 1, section 3.2, has an inherent subjective element. As one of the main goals of this report is to aid the process of eliminating subjective elements regarding the evaluation of material properties, it is of great importance that these results are reliable if further assumptions surrounding the connection between ductility and the grade of cracking are to be made. Our results will to a degree be compared with those of Parson et al. [9], [15], as they have done more extensive research on the subject, however regarding more alloys and crash boxes with a simpler geometry. As seen in Figure 14, the degree of cracking seems dependent on the absolute ductility of the metal, represented by the true fracture strain, rather than the processing parameters. This speaks volumes about the probability of being able to predict the

cracking behaviour of a crash box through a simple tensile test. However, compared to the results of Parson et al., our results point toward a linear relationship with a decreasing degree of cracking with higher true fracture strain, eventually reaching crack-free boxes, while their result points at there being a threshold value of a true fracture strain of 0.7 that if surpassed, causes soft alloyed aluminium crash boxes to crack [9]. Consequently, there is reason to believe that there are relevant correlations to be found but that they may be connected rather to the geometry and the alloying composition of the crash boxes, not treated in this report. Further research is required to fully establish working evaluation models for crash boxes with certain geometries and compositions. It is however fairly safe to conclude that cracking behaviour may be predicted through similar modelling using true fracture strain and equivalently, the area reduction Z when regarding the 6063-alloy.

5.1.3 Evaluation of ductility parameters

Serving the purpose of this report, the determination of which parameters may be used to evaluate the ductility of an aged alloy in relation to its strength has been evaluated following Figures 16 through 18. In the internal study at Hydro Extrusion Sweden AB by Assisi [14], the increase of Z , true fracture strain and R_m-R_f proved to correlate with the decrease of strength for longer ageing times, Z and true fracture strain better than R_m-R_f . Based on Assisi's results, the three same parameters were evaluated in this study, however this time including air-cooled samples. Assisi's results were clear, with all the discussed parameters suitable to evaluate the ductility of samples. However, based on Figures 16 through 18, the case is not as clear with respect to our result, partly because of the great standard deviation of some samples. Because of the results following Assisi, Z and true fracture strain are to be considered good parameters used to evaluate ductility. This includes both water-quenched and air-cooled samples, as the curves follow a similar trend in Figures 16 and 17 but most importantly, as their correlation displayed in Figures 19 a) through 22 b), discussed in the following paragraph, hold R^2 values greater than 0.8 for all over aged samples and R^2 values greater than 0.7 for underaged samples. Regarding the trustworthiness of R_m-R_f as a ductility parameter, the standard deviations are too large to be considered acceptable.

5.1.4 The relation between ductility, strength and ageing time

Figures 19 a) through 24 b) represent the correlation of ductility and strength of tensile test samples dependent on the ageing cycles. As discussed by Assisi [14] and shown here with all the mentioned Figures ending with "a)", the correlations between over aged samples are very strong with a coefficient of determination R^2 greater than 0.95, with the exceptions where R_m-R_f have been used as the ductility parameter. Similarly, the correlations represented in all the mentioned Figures ending with "b)" for over aged and under aged samples, both including peak-aged samples, are generally good with the coefficient of determination ranging from $R^2=0.77$ to $R^2=0.99$; with the exception of water-quenched samples evaluated with

R_m-R_f . Conclusively, this proves how well ductility and strength may be modelled with respect to ageing and, as mentioned in the previous paragraph, that R_m-R_f as a ductility parameter may be uncertain with this small amount of data.

A general trend observed shows that under aged samples approaching peak-ageing as well as over aged samples close to peak ageing when plotted seem to form an acute angle, with the peak-aged sample at the very point. This represents the fundamental relationship that high strength comes at the cost of ductility and vice versa, which is independent of the quenching method. Generally, we may observe that over aged samples serve the best properties when both strength and ductility are required, further confirming the thesis presented by Morita et al. [8] and Parson et al. [9].

Regarding the difference in strength when comparing the two quenching methods for the same ageing cycle, it seems to be abnormally small, no matter if we regard $R_{p0.2}$ or R_m . The abnormality of this difference was brought up through the same discussion with Altzar and Assisi mentioned in 5.1.1. However, following the results of Parson [9], we still observe a higher level of ductility for a set level of strength for water quenched samples which is more interesting with regards to our purpose.

5.1.5 Correlation between MCF and R_m , MCF and $R_{p0.2}$

Figure 15 shows the strong correlations between MCF and $R_{p0.2}$ and between MCF and R_m . The study by Parson et al. performed the same kind of plots [9], but their study included several alloys and a broader range of ageing cycles. Similar to Parson et al., Figure 15 shows a strong relationship between R_m and MCF for both water and air-quenched samples. However, in our plots, it looks like there are linear relationships between $R_{p0.2}$ and MCF too, but assumptions may be treacherous due to the low amount of points for both over and under aged samples. Parson et al. got a bent curve with a distinction between under- and over aged samples, in this study, however, the points in the graph are probably too few.

5.1.6 Correlation between R_m-R_f and Z

According to Figure 25, the relationships between R_m-R_f and Z are approximately linear, independent of the cooling method or ageing cycle, with the exception of T4-samples that do not correlate whatsoever with the other samples. Nevertheless, as presented in Tables 3 and 4, standard deviations regarding R_m-R_f are often large, rendering the regressions of Figure 25 untrustworthy despite the R^2 -values around 0,9. Likewise, this relation has been shown by Assisi to exist for similar aged and water-quenched soft aluminium alloys with similar standard deviations [14]. This, due to the similarities of our water-quenched and air-cooled samples, although with large standard deviations, may lead one to believe that the same relationship may exist for air-cooled samples. However, one of the conclusions drawn by Assisi points out that this correlation needs to be evaluated with larger data sets before any

conclusions can be drawn that the measuring of Z can be replaced by R_m-R_f . Assisi used four samples for each point of cooling method- and ageing combination [14] and despite the recommendation to use a larger set of data, we have only used three samples per process iteration. This follows the limitations of our project, as at least two ageing programs on both sides of the peak ageing point were prioritised before having a large amount of data for every cooling method and ageing cycle combination. Note that an established relation between R_m-R_f and Z could, within the certain limits presented by alloy and processing parameters, enforce R_m-R_f as a proper measurement of ductility. Further allowing operators to predict the cracking behaviour of a crash box by inspecting R_m-R_f directly in the graph following a tensile test.

It is interesting to note that the unaged samples did not follow this trend at all, since the T4 samples showed a very ductile behaviour both when it came to area reduction and cracking behaviour. But in the aged samples, Mg_2Si precipitates probably formed during ageing [16]. Therefore the forming and coalescence of voids may have occurred during necking in the aged samples [21]. A speculation around that is that the cup and cone fracture gives indications from the tensile test machine further in the necking progress due to the resistance of precipitations and voids hindering dislocations to move.

5.2 Comments on production and measurement methods

The measurements of the cooling rate went quite well overall. Billet 2 showed, however, a bit higher cooling rate than billet 3 as billet 2 had a quite slower extrusion rate than the other billets, which gave the profile more time in the quench box. It should be pointed out that the difference in cooling rate between billet 2 and 3 is large and may have influenced the results in a way that we have not taken into account. The cooling curve for billet 4 is more uneven than the others which may be explained by variation in voltage that may have occurred between the contact spots of the fork thermocouple.

Sawing up compression sample pieces from the profiles was not done with much precision, the samples intended to be used for compression testing were thought to be 300 mm, but the difference between pieces showed to differ a few centimetres after sawing was done.

An observation from the compression test was that the specimens were hot directly after compression, suggesting that some energy from the compression test had been transformed into heat.

The determination of the grade of cracking was not easy to perform in a way that seemed fully accurate since there is no widely standardised method available. The method that was finally decided to be used was chosen late in the process when only

pictures of the samples were available where not all sides of the samples were visible. Grading whilst having access to the samples would have been preferable. The method used by Parson et al. differed from the method used here both in terms of crack grade evaluation method and profile form. In the study by Parson et al., the profile is a simple rectangular tube while the profile used in this study has inner walls. Parson also used an initiation for the folding to get more homogeneous results in the crash force measurements [9]. The cracking occurred mostly in the T-joints between inner and outer walls which makes the comparison with results from the studies by Parson et al. somewhat difficult.

The area reduction measurements with help from the microscope were done in a similar manner as in the internal investigation by Assisi. The report from the investigation states that this method went well [14]. With the help of the aforementioned computer program with a drawing tool and automatic calculation of area, it was possible to follow the sometimes very irregular outlines of the fracture surface. In many cases, the microscope pictures gave a good view of the lines but sometimes it was hard to see if the drawing was done in the right places, so in some cases this measurement became arbitrary, but overall it went well. However, this is a time-consuming method. Unluckily the pictures displayed in Figures 6 through 12 and Appendix B, were accidentally saved without a scale.

Regarding the statistical certainty of all the parameters and related correlations that do not derive from the measurements of the tensile tests samples' fracture areas, there is an important comment to make. Both the tensile- and compression testing have been performed using equipment in an industrial setting. Therefore, the results deriving from this equipment can not secure exact measurements. Consequently, correlations formulated with these parameters may not be considered absolute, but rather as indications of trends that may be proven in a lab-setting with larger sets of data.

5.3 The Aluminium industry and CO₂ emissions

As mentioned in the introduction of this report, the use of aluminium in the vehicle industry is expected to increase in the near future [2]. With the high strength-to-density ratio and the great recyclability of aluminium, the use of aluminium, compared to other metals, may help to minimise the required energy to drive the cars while enabling easier and less energy-costing recycling processes at the end of the life cycle for a larger fraction of the car's bodies. But with an increased use of aluminium comes more challenges, since an increase in aluminium demand will increase the need for virgin aluminium. The production of primary aluminium causes large CO₂ emissions. A great part of the total emissions stems from fossil fuel-based electrical energy that is needed for electrolysis and bauxite processing. The transfer to exclusively fossil-free electricity would be a solution to reduce CO₂ emissions, but that is a goal which is hard to achieve because of the very high

demand for green energy. Another major source of emissions comes from the carbon anodes themselves during the electrolysis process. There is ongoing research with the aim of developing an inert anode that will cause O₂-emissions during the reaction instead of CO₂. New and more strict climate policies could contribute to the development of aluminium production with less emission, but then there is a risk of so-called carbon leakage, which is when companies move their operation to other countries with less strict CO₂-policies [23]. The type of research presented in this report could contribute to the development of the production of aluminium construction details and thus contribute to the increasing amount of aluminium in vehicles. Therefore it is important to keep the sustainability aspects of aluminium production in mind when proceeding and adapting this research.

6. Conclusions

Based on the results of this report, conclusions may be stated as follows:

- A linear correlation has been observed between area reduction Z and the difference $R_m - R_f$ for both water- and air-quenched samples. However, no reliable relationship where $R_m - R_f$ is used as a ductility parameter has been found because of the high standard deviations, small coefficients of determination and an unreliable trend of increased ductility with increased ageing time.
- Air-cooled samples resulted in lower area reduction and were more prone to cracking at lower MCF than water-quenched samples.
- A linear correlation can be observed between MCF and R_m as well as between MCF and $R_{p0.2}$. The latter contradicts the results of previous studies with much larger data sets and variations in ageing and alloys [9]. Thus, the correlation between MCF and R_m is to be considered more reliable, however, a larger set of data points is needed to confirm accuracy.
- Regarding an over aged 6063-alloy, it may be possible to predict the cracking behaviour of a crash box with respect to ductility and ageing if a proper model is used. Based on our results and those of Parson et al., [9] the model used should be adjusted to the geometry of the crash box.
- There are strong indications that the increase of ductility of an over aged 6063-alloy, evaluated from area reduction Z or calculated true fracture strain, linearly correlates with the loss of strength for a longer ageing time no matter if the alloy has been water-quenched or air-cooled.

7. Recommendations

For similar future work, the recommendations would be to use a larger set of data for every combination of alloy and production parameters to be able to draw more accurate conclusions from the found correlations. Also to include more ageing cycles, especially several under aged samples in order to solidify the correlation between strength, ductility and ageing. It would be interesting to also investigate several alloys, especially alloys with higher alloying content that do not fully recrystallise.

During the evaluation of the grade of cracking the recommendation is to formulate a grading scale and strategy early in the research progress and do the final grading whilst having access to the physical samples. Generally, there is a need to unravel some uncertainties around how much the geometry of the profile affects the correlation between the degree of cracking and ductility. Greater clarity on this point would broaden the possibilities to compare the results of different studies handling different kinds of crash boxes.

During compression testing, it would maybe be interesting to record with a thermal camera, as the temperature during compression may be an interesting parameter relating to energy absorption.

Furthermore, as the measurements of R_m - R_f resulted in large standard deviations while true fracture strain and degree of area reduction did not, we recommend trying to automatise the measuring of the fracture surface areas. We believe that this may be one of the most effective methods to circumvent the need for compression tests.

8. Acknowledgements

We would like to express our deepest gratitude to Hydro Extrusion Sweden AB for the opportunity to write our bachelor thesis in collaboration with them. Also to all the employees at Hydro in Finspång who assisted us by managing production and testing equipment, we say thank you. Without their help and patience, this project would not have been possible.

We would especially like to express our gratitude to our external supervisor Oskar Altzar, process engineer at Hydro Extrusion Sweden AB, Vetlanda, who initially formulated the thesis and who has aided us tremendously throughout the entire time of our project. Furthermore, we would like to thank Henrik Lindberg, trainee at Hydro Extrusion Sweden AB, Finspång, who along with Oskar Altzar helped us during our visits to the plant in Finspång with the execution of the experimental elements of this study.

The thesis of this study is based upon the work of Andreas Assisi, project manager at Hydro Extrusion Sweden AB, Finspång, often referenced in this report. We also express our gratitude towards him as he has provided great aid with the understanding of relevant concepts.

Likewise, we would like to express our deepest gratitude towards our academic supervisor, Professor Stefan Jonsson of the unit of properties, Department of Material Science and Engineering at KTH Royal Institute of Technology, Stockholm, Sweden, for his expertise surrounding the mechanical properties of metallic materials and great encouragement. Moreover, we would like to thank the course examiner and director of studies at the Department of Material Science and Engineering, KTH Royal Institute of Technology, Anders Eliasson, for academic guidance and help with the structure of this report.

9. References

- [1] H. Zhong, P. A. Rometsch, and Y. Estrin, 'The Influence of Alloy Composition on the Microstructure, Tensile Ductility and Formability of 6xxx Alloys', in *ICAA13 Pittsburgh*, H. Weiland, A. D. Rollett, and W. A. Cassada, Eds., Cham: Springer International Publishing, 2016, pp. 687–692. doi: 10.1007/978-3-319-48761-8_100.
- [2] Ducker Research & Consulting, 'Aluminum Content in Passenger Vehicles (Europe)', Apr. 2023.
- [3] J. Mendoza, 'Literature study: Possible correlations between microstructure, tensile properties, formability and crashworthiness of aluminium alloys', Unpublished, May 2014.
- [4] N. N. Hussain, S. P. Regalla, Y. V. D. Rao, T. Dirgantara, L. Gunawan, and A. Jusuf, 'Drop-weight impact testing for the study of energy absorption in automobile crash boxes made of composite material', *Proc. Inst. Mech. Eng. Part J. Mater. Des. Appl.*, vol. 235, no. 1, pp. 114–130, Jan. 2021, doi: 10.1177/1464420720952813.
- [5] 'This is Hydro'. Accessed: May 06, 2024. [Online]. Available: <https://www.hydro.com/en/about-hydro/this-is-hydro/>
- [6] 'Sweden'. Accessed: May 06, 2024. [Online]. Available: <https://www.hydro.com/en/about-hydro/hydro-worldwide/europe/sweden/>
- [7] 'Hydro Extrusions Finspång'. Accessed: May 06, 2024. [Online]. Available: <https://www.hydro.com/en/about-hydro/hydro-worldwide/europe/sweden/finspang/hydro-extrusions-finspang/>
- [8] K. Morita, S. Yoshihara, and T. Oka, 'Effect of Microstructure on Crack of Al-Mg-Si Alloy Extrusions during Axial Compression', *Mater. Sci. Forum*, vol. 519–521, pp. 895–900, Jul. 2006, doi: 10.4028/www.scientific.net/MSF.519-521.895.
- [9] N. Parson, J. Fourmann, and J.-F. Beland, 'Aluminum Extrusions for Automotive Crash Applications', presented at the WCX™ 17: SAE World Congress Experience, Mar. 2017, pp. 2017-01–1272. doi: 10.4271/2017-01-1272.
- [10] A. Vazdirvanidis *et al.*, 'Examination of Buckling Behavior of Thin-Walled Al-Mg-Si Alloy Extrusions', in *ICAA13 Pittsburgh*, H. Weiland, A. D. Rollett, and W. A. Cassada, Eds., Cham: Springer International Publishing, 2012, pp. 909–914. doi: 10.1007/978-3-319-48761-8_136.
- [11] M. Rosefort, R. Baumgart, C. Matthies, and H. Koch, 'Influence of Microstructure on the Folding Behavior of Crash Relevant Aluminum Extrusion Parts', in *Light Metals 2014*, 1st ed., J. Grandfield, Ed., Wiley, 2014, pp. 201–205. doi: 10.1002/9781118888438.ch35.
- [12] J. Datsko and C. T. Yang, 'Correlation of Bendability of Materials With Their Tensile Properties', *J. Eng. Ind.*, vol. 82, no. 4, pp. 309–313, Nov. 1960, doi: 10.1115/1.3664236.
- [13] R. Stevenson, 'Correlation of tensile properties with plane-strain, limiting dome height', *J. Appl. Metalwork.*, vol. 3, no. 3, pp. 272–280, Jul. 1984, doi: 10.1007/BF02833655.
- [14] A. Assisi, 'Technical memo - Overaging 6063 - Effect on ductility measured as area reduction Z', 12 aug 2021, Unpublished.
- [15] N. Parson, J. Fourmann, and J.-F. Béland, 'Extrusions for Automotive Crash Applications', Unpublished, 2016.
- [16] I. Polmear, D. StJohn, J.-F. Nie, and M. Qian, 'Wrought Aluminium Alloys',

- in *Light Alloys Metallurgy of the Light Metals*, Fifth edition., Elsevier Ltd., 2017. [Online]. Available: <https://11nq.com/VxoKN>
- [17] T. Sheppard, *EXTRUSION OF ALUMINIUM ALLOYS*, 1st ed. Department of Product Design and Manufacture, Bournemouth University: Springer Science + Business Media Dordrecht, 1999.
- [18] 'SVENS K STANDARD SS-EN 573-3:2019 - [PDF Document]', documents.pub. Accessed: Mar. 01, 2024. [Online]. Available: <https://documents.pub/document/svens-k-standard-ss-en-573-32019.html>
- [19] O. Altzar, 'Gästföreläsning Hydro Sweden AB', Finspång, Sweden, Feb. 22, 2023.
- [20] Nick Parson: *Automotive Extrusions with Improved Strength and Ductility - YouTube*, (Jul. 20, 2018). Accessed: Apr. 05, 2024. [Online Video]. Available: <https://www.youtube.com/watch?v=ldO6BLTb4kk>
- [21] S. Jonsson, *Mechanical Properties of Metals and Dislocation Theory from an Engineer's Perspective*. Stockholm, 2010.
- [22] M. F. Ashby, H. Shercliff, and D. Cebon, *Materials: engineering, science, processing and design*, Fourth edition. Kidlington, Oxford, United Kingdom ; Cambridge, MA, United States Amsterdam: Butterworth-Heinemann is an imprint of Elsevier, 2019.
- [23] G. Saevarsdottir, H. Kvande, and B. J. Welch, 'Aluminum Production in the Times of Climate Change: The Global Challenge to Reduce the Carbon Footprint and Prevent Carbon Leakage', *JOM*, vol. 72, no. 1, pp. 296–308, Jan. 2020, doi: 10.1007/s11837-019-03918-6.

Appendix

Appendix A: Microscopy images



Fig. A1, 165/6h water-quenched.

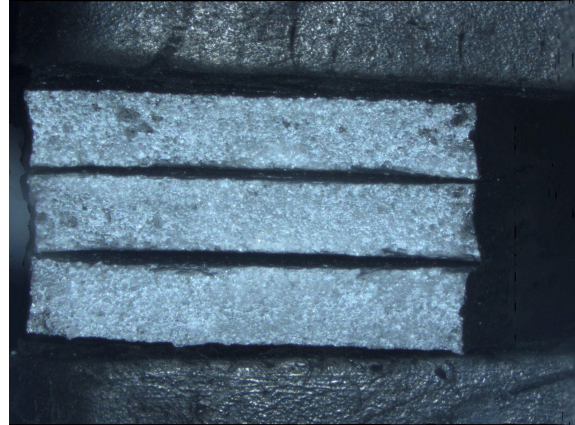


Fig. A2, 165/6h air-cooled.

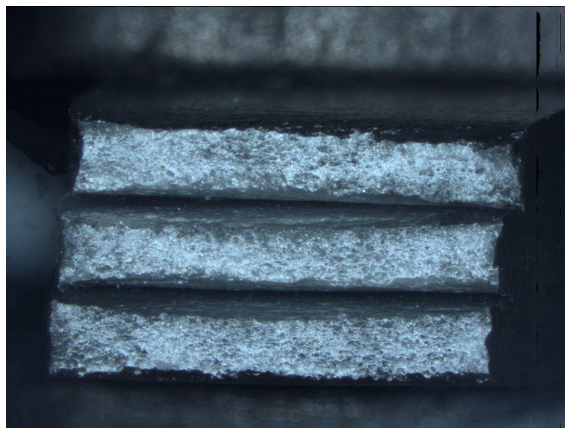


Fig. A3, 215/1h water-quenched.

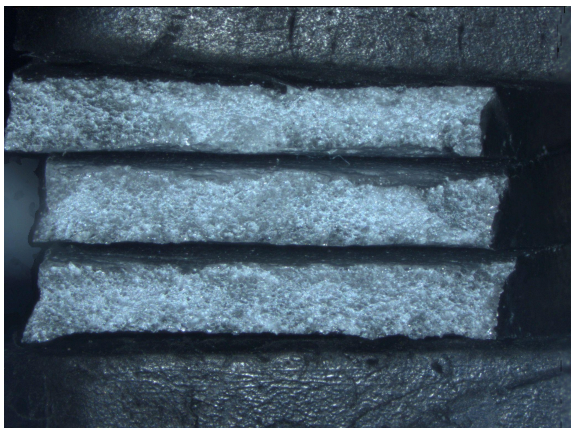


Fig. A4, 215/1h air-cooled.

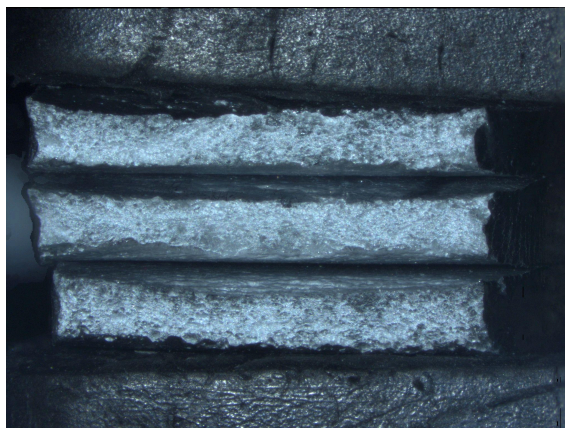


Fig. A5, 215/2h water-quenched.

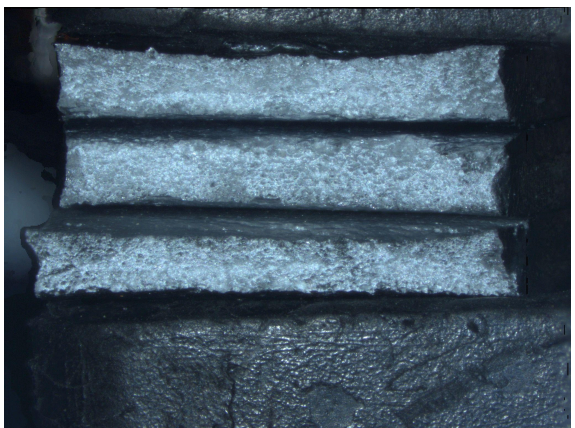


Fig. A6, 215/2h air-cooled.

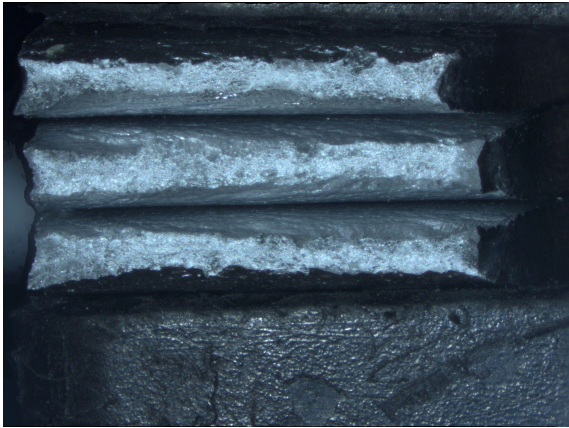


Fig. A7, 215/4h water-quenched.

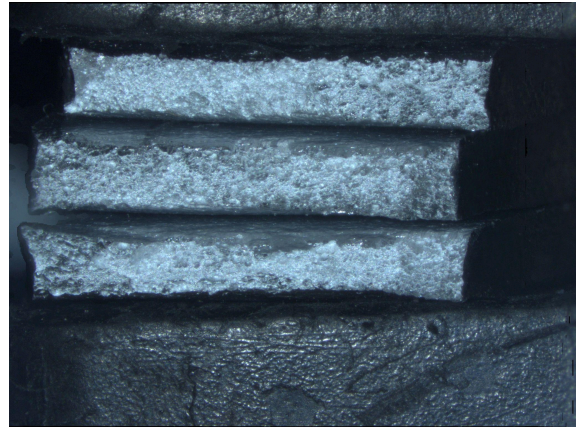


Fig. A8, 215/4h air-cooled.

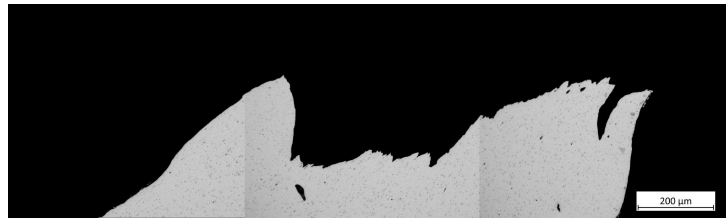


Fig. A9, the fracture surface of the second picture of a tensile test sample that has been water-quenched and aged for 6h at 215°C.

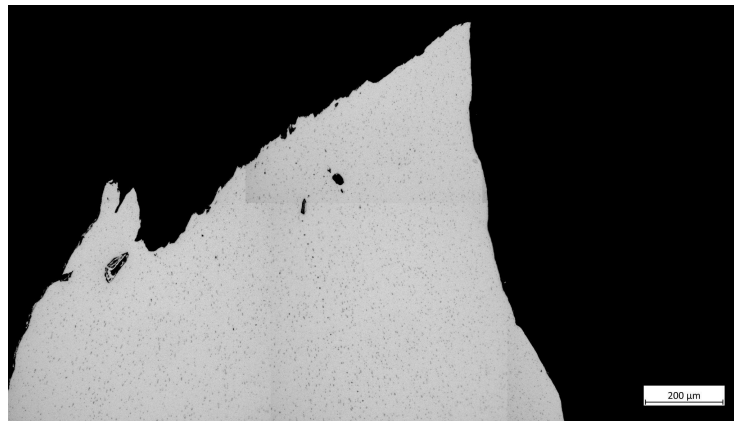


Fig. A10, the fracture surface of the third picture of a tensile test sample that has been water-quenched and aged for 6h at 215°C.

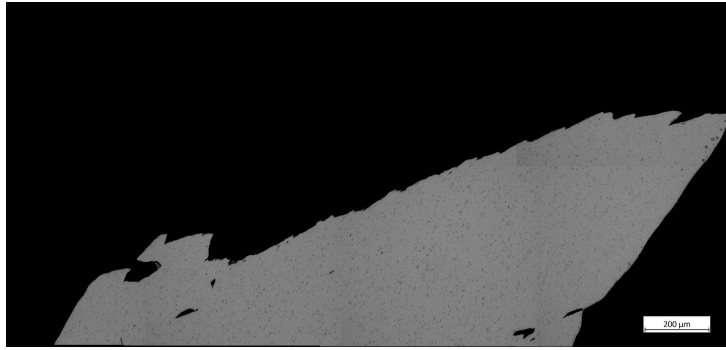


Fig. A11, the fracture surface of the second picture of a tensile test sample that has been air-cooled and aged for 6h at 215°C.

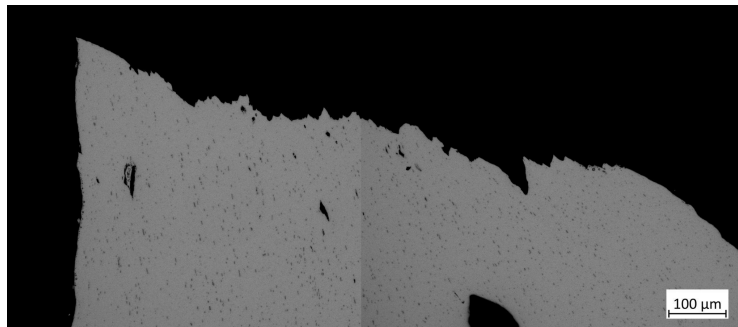


Fig. A12, the fracture surface of the third picture of a tensile test sample that has been air-cooled and aged for 6h at 215°C.

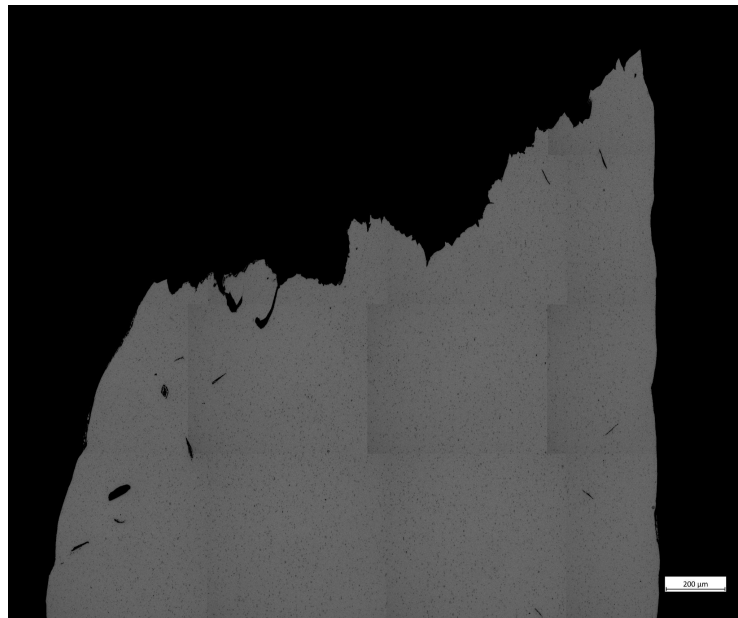


Fig. A13, the fracture surface of the first tensile test sample that has been water-quenched and peak-aged.

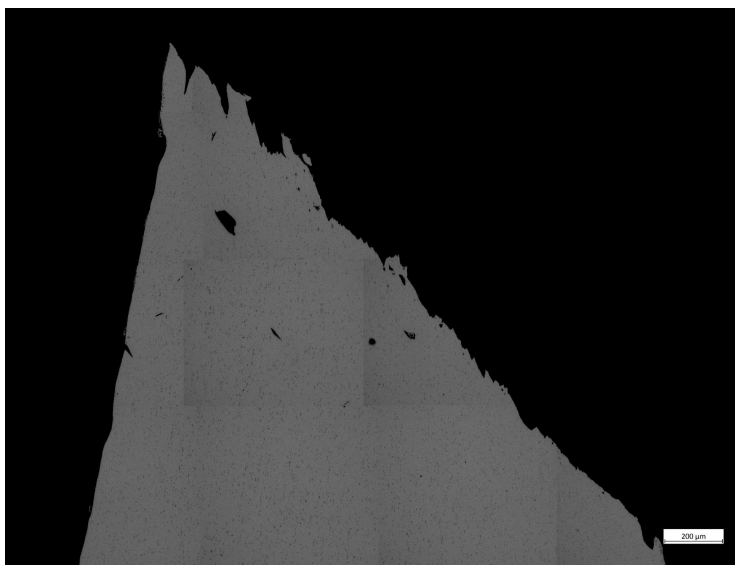


Fig. A14, the fracture surface of the second tensile test sample that has been water-quenched and peak-aged.

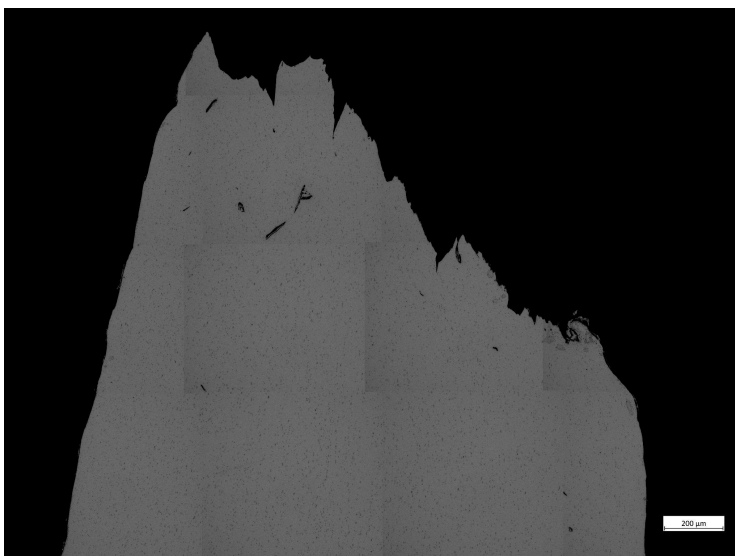


Fig. A15, the fracture surface of the third tensile test sample that has been water-quenched and peak-aged.

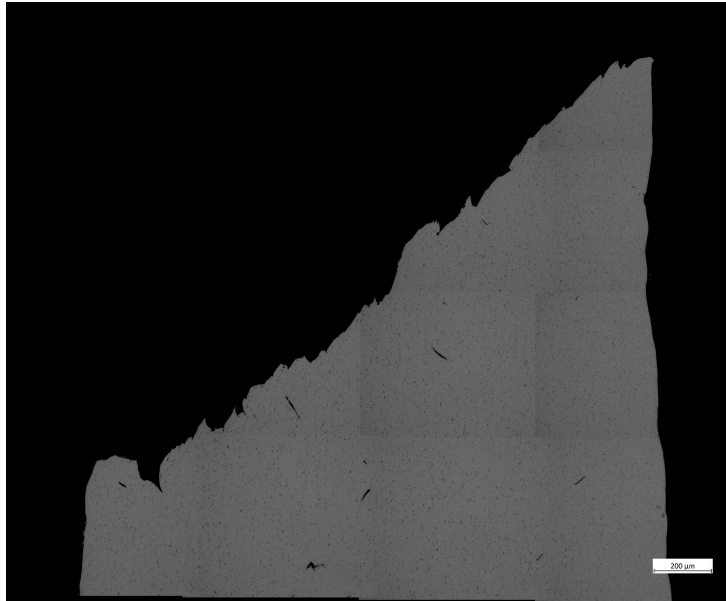


Fig. A16, the fracture surface of the first tensile test sample that has been air-cooled and peak-aged.

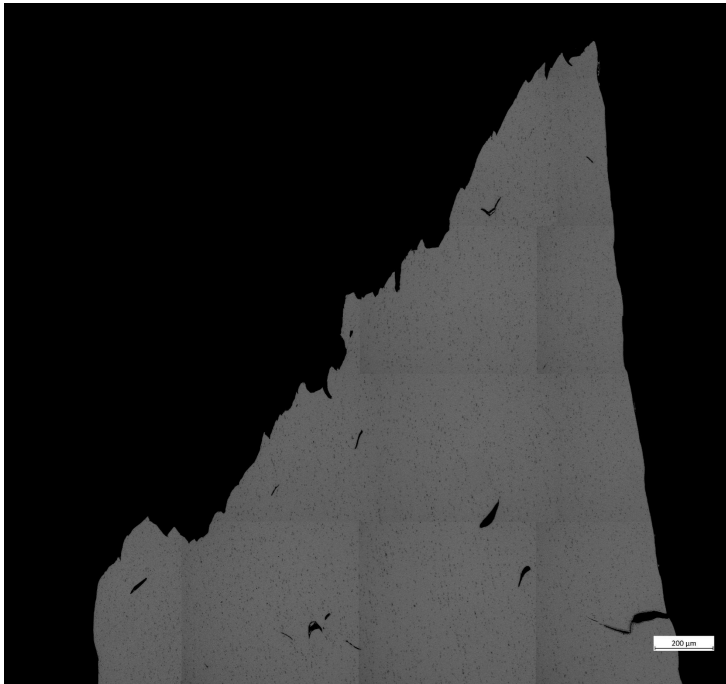


Fig. A17, the fracture surface of the second tensile test sample that has been air-cooled and peak-aged.

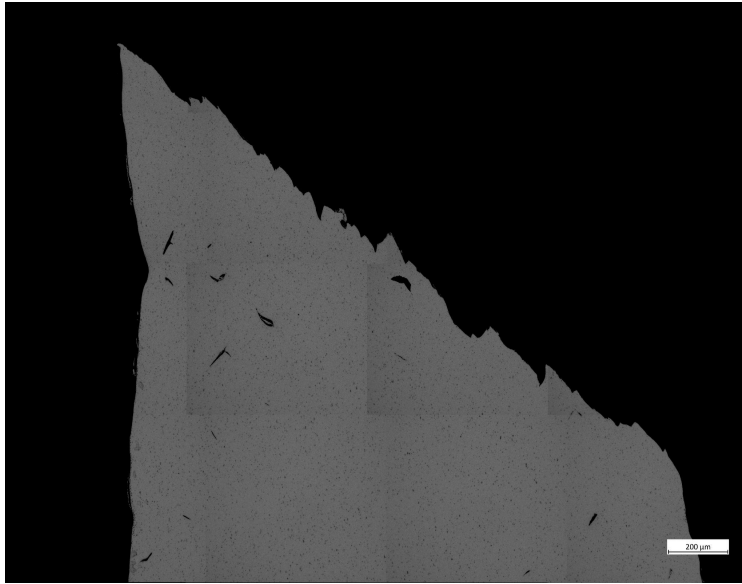


Fig. A18, the fracture surface of the third tensile test sample that has been air-cooled and peak-aged.

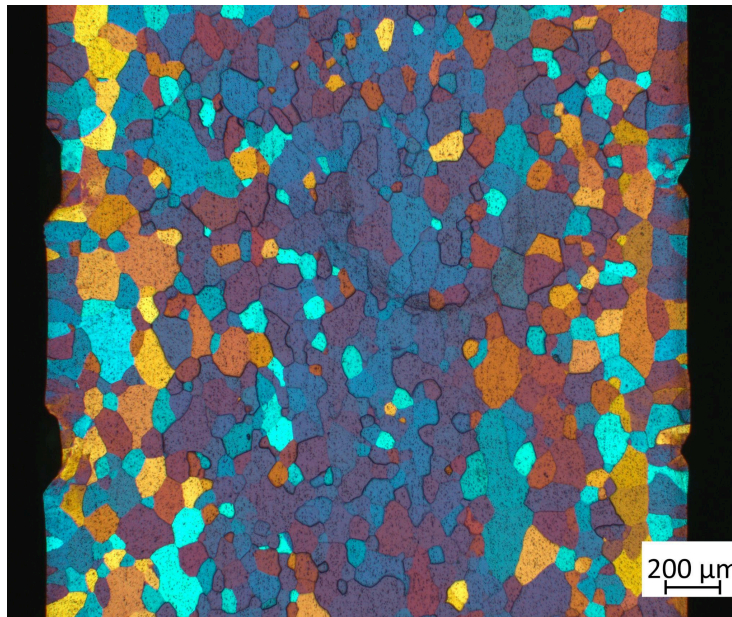


Fig. A19, the microstructure of a water-quenched and peak-aged sample that has been taken parallel to the extrusion direction.

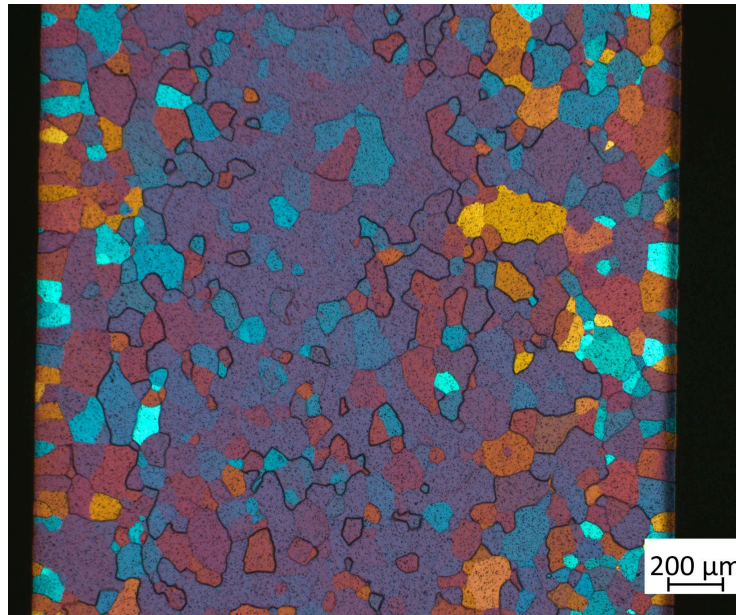


Fig. A20, the microstructure of a water-quenched and peak-aged sample that has been taken perpendicular to the extrusion direction.

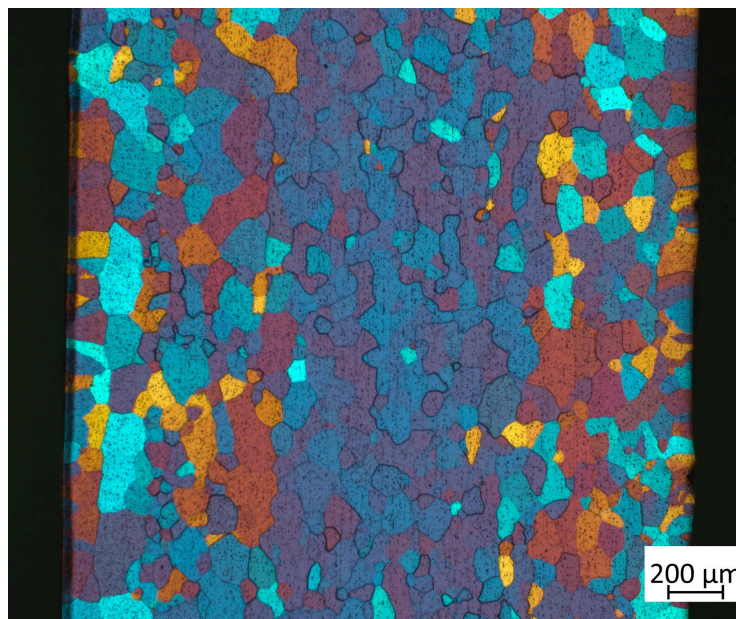


Fig. A21, the microstructure of an air-cooled and peak-aged sample that has been taken parallel to the extrusion direction.

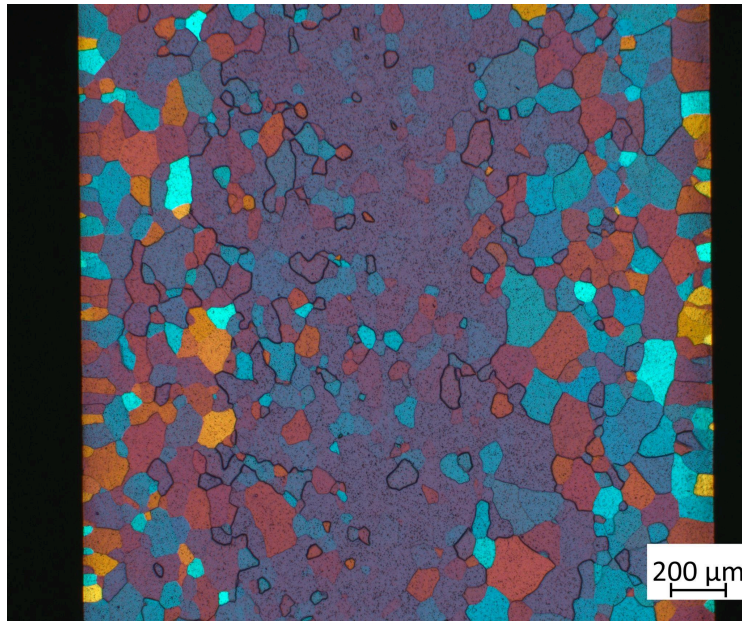


Fig. A22, the microstructure of an air-cooled and peak-aged sample that has been taken perpendicular to the extrusion direction.

